



Graphical Representation and Explanation of the Conductivity Tensor of Anisotropic Media

Chang-fu Yang¹ · Lin-jiang Qin^{2,3}

Received: 25 November 2018 / Accepted: 14 December 2019 / Published online: 29 January 2020
© Springer Nature B.V. 2020

Abstract

Electrical anisotropy is a property of the Earth materials that can be studied through electromagnetic geophysical methods, such as magnetotellurics. It consists of the electrical conductivity changing with the orientation and being mathematically characterized by the conductivity tensor. In order to better understand the conductivity tensor and provide more effective tools for quantitatively analyzing the conductivity tensor of anisotropic structures, three graphical representations for symmetric tensors using ellipsoids, Mohr circles and geometric forms are presented. The ellipsoid representation can be applied to indicate the strength of the anisotropy in different directions. The Mohr circle provides a graphic representation of a tensor as a function of the rotation of the coordinate system. For the geometric forms, one-dimensional (1-D), two-dimensional (2-D) and three-dimensional (3-D) sheet models with given parameters (sizes and resistivities of the constituent prisms), the macroscopic anisotropic conductivity may be calculated using the closed-form mathematical formulas. These three graphical representations have different abilities for revealing information on the conductivity tensor. Four synthetic examples involving uniaxial or biaxial anisotropic conductivity structures are examined in the principal axis coordinate system to investigate the advantages and disadvantages of the graphical displays.

Keywords Anisotropy · Conductivity tensor · Graphical representation · Ellipsoid of conductivity tensor · Mohr circle · Model of conductivity tensor

✉ Chang-fu Yang
ycffc6422@sina.com; ycfzju@zju.edu.cn

Lin-jiang Qin
qinlinjiang@126.com

¹ School of Earth Sciences, Zhejiang University, Hangzhou 310027, China

² Key Laboratory of Submarine Geosciences, Ministry of Natural Resources, Hangzhou 310012, China

³ Second Institute of Oceanography, Ministry of Natural Resources, Hangzhou 310012, China

1 Introduction

It is an indisputable fact that the conductivity structure of the crust and the upper mantle in the Earth is electrically anisotropic to some extent. Electrical anisotropy has attracted widespread attention from the scientists in geophysical electromagnetics. Many magnetotelluric (MT) experiments related to electrical anisotropy have been carried out to map the conductivity structures in the lithospheric and upper mantle on land (Regis and Rijo 1997; Eisel and Haak 1999; Bahr and Duba 2000; Regis and Rijo 2000; Miensopest and Jones 2011; Adetunji et al. 2015) and in marine environments (Everett and Constable 1999; Baba et al. 2006; Meju et al. 2018). Much progress has been made in development of forward algorithms for anisotropic structures (Pek and Verner 1997; Yang 1997; Li 2002; Løseth 2007; Qin et al. 2013; Qin and Yang 2016), in development of inversion techniques (Regis and Rijo 2000; Yin 2000, 2003; Pek and Santos 2006; Mandolesi and Jones 2012) and in examination of the effect of anisotropy on MT transfer functions (Weidelt et al. 1999; Heise et al. 2006) as well as the dimensionality analysis (Santos and Mendes-Victor 2000; Martí et al. 2010; Martí 2014; Okazaki et al. 2016; Löwer and Junge 2017). There are also many studies involving resistivity anisotropy in the fields of the DC resistivity (Maillet 1947; Montgomery 1971; Sasaki 1994; Yin and Weidelt 1999; Pain et al. 2003; Herwanger et al. 2004; Greenhalgh et al. 2009; Wiese et al. 2015; Falae et al. 2019) and in geophysical well logging (Moran and Gianzero 1979; Wang and Fang 2001; Weiss and Newman 2002) as well as in the rock physics studies (Du Frane et al. 2005; Pommier 2014; Börner et al. 2018). Additionally, it is worth mentioning that the anisotropic conductivity has an important role in medical imaging. For example, it has been shown that the electrical conductivity of the white matter in the brain and the skeletal muscle exhibits strong anisotropy (Holder 2004; Jeong et al. 2017), and many researchers proposed different methods to reconstruct anisotropic conductivity tensor images (Sen and Torquato 1989; Seo et al. 2004; Kwon et al. 2014; Jeong et al. 2017).

The conductivity tensor, which can be used to characterize the anisotropic electrical properties of the rocks in the Earth, is an essential physical parameter to be considered in the electromagnetic induction in Earth. Hence, it is crucial to understand the conductivity tensor.

In space physics, the influence of the geomagnetic field \mathbf{B} on the charged particles in the atmosphere will cause the Hall effect, which may lead to the existence of the Hall conductivity (Onwumechilli 1967; Rokityansky 1982; Takeda and Masahiko 1991; Kittel 2005; Rastogi and Chandra 2006; Chapagain 2016). In addition, there are still the Cowling conductivity (Cowling 1945; Atkinson 1967) and Pedersen conductivity (Le et al. 2010) in Earth's ionosphere. In this environment, the conductivity tensor is antisymmetric rather than symmetric as would be in the case of crystals (Baker and Martyn 1953). In some special cases, the Hall current in the Earth cannot be ignored. For example, the host rocks above the deposits of oil and gas can be considered a semiconductor medium in which the Hall effect may occur (Gololobov and Malevich 2005; Plotkin 2017).

In general, the Hall conductivity, the Cowling conductivity and the Pedersen conductivity are all ignored in studies of the Earth's crust and mantle, and the dispersion effect (the variation in the conductivity with the frequency of the electromagnetic signal) is also ignored, i.e., it is also necessary to neglect the imaginary component of conductivity associated with electrical polarization in order to treat the conductivity as a purely real quantity. Under these circumstances, the anisotropic conductivity tensor in the rock of the Earth is symmetric (a proof of that can be found in Dekker and Hastie 1980, Appendix C). Then,

the anisotropic conductivity tensor is symmetric positive and definite, which is similar to the case of crystal (Feynman et al. 1965). Therefore, the properties of the crystal conductivity tensor can be extended to the anisotropic medium in Earth, so some properties and illustrations of the crystal symmetry tensor (Nye 1985) can also be analogized or extended to the tensor in Earth medium.

Graphical representation for symmetric tensors is a quite intuitive and effective way to help people correctly understand anisotropy. In physics, the graphical representation for symmetric tensors is usually carried out by three ways, i.e., by ellipsoids and Mohr circles as well as equivalent geometric forms. The graphical representations of the conductivity tensor using ellipsoids are discussed in some textbooks in which the physical properties of the crystal are described with tensors (Nye 1985; Kittel 2005). The second graphical representation of conductivity tensors—Mohr circle which was first introduced by Culmann (1866) and further by Mohr (1882) and then was used to represent the stress tensor by Jaeger (1969) in elastic mechanics—will be introduced in this work. In geo-electromagnetics, relatively less attention is paid on the graphical representation of the conductivity tensor in anisotropic media by ellipsoids and Mohr circles. Mohr circle is introduced by Lilley (1976) and other authors (Makris et al. 1999; Weaver and Lilley 2004) to represent the MT impedance tensor rather than conductivity tensor. However, no publications have reported the use of Mohr circle representation of the conductivity tensor.

More attention has been paid to the relationship of geometric forms representing anisotropic media and the corresponding conductivity tensor. For example, physical realizations of several media characterized by a uniaxial electrical conductivity tensor in which one of the three components of the conductivity tensor in the principal axis coordinate system is different from the other two were presented by Everett and Constable (1999), who also illustrated several simple conductivity tensor models by geometric forms. Many other authors have carried out similar work (e.g., Maillet 1947; Grant and West 1965; Mollison et al. 1999; Schön et al. 1999; Wannamaker 2005). For biaxial anisotropic conductivity (e.g., Mogilatov and Bepalov 2009), also known as triaxial anisotropic conductivity in some literature (e.g., Nekut 1994), which has different conductivity values along all three principal axes, the anisotropic conductivity tensor has been represented in terms of 2-D or 3-D random networks and corresponding formulas by some authors (e.g., Madden 1976; Schmeling 1986; Bahr 1997; Pervukhina et al. 2005; Kirkby and Heinson 2017). However, the geometric representation of anisotropic models that these authors have given is relatively complicated and inconvenient to be applied to test modeling and inversion programs. Therefore, we will provide some simpler geometric forms and straightforward formula to calculate the macroscopic conductivity tensor for several simple anisotropic models.

It is beneficial to understand the properties of the electrical anisotropy in the Earth when a more general conductivity tensor is represented with a simple geometric model. Therefore, a link between the 2-D or 3-D isotropic and macroscopic anisotropic conductivity models may be established, and the diagonal elements of the general macroscopic conductivity tensor in the principal coordinate system can be represented in terms of parameters of isotropic model (sizes and conductivities of the constituent elements) through the mathematical expression, which provides a more convenient tool for quantitatively studying the anisotropic properties of the Earth medium.

The structure of this paper is as follows: The definition of the conductivity tensor of anisotropic media in geo-electromagnetism is summarized in Sect. 2. Section 3 describes the representation of the conductivity tensor under the rotation of the coordinate system. Subsequently, three graphical representations of the anisotropic conductivity tensor, i.e., the 3-D ellipsoid, the Mohr circle diagrams and geometric forms, are

illustrated in Sects. 4, 5 and 6, respectively. Then, in Sect. 7, for the geometric model with given parameters, the macroscopic anisotropic conductivity is calculated using the closed-form mathematical formulas in Sect. 6; then, three graphical presentations of these calculated anisotropic conductivity tensors are presented as synthetic examples. Finally, the work is closed with some discussions in Sect. 8 and conclusions in Sect. 9.

2 The Definition of the Conductivity Tensor

In an anisotropic medium, the relationship between the conductivity, current density and electric field strength can be expressed by Ohm’s law:

$$\mathbf{J} = \boldsymbol{\sigma}\mathbf{E}^T \tag{1}$$

where \mathbf{J} is the current density vector and $\boldsymbol{\sigma}$ represents the conductivity tensor, and $\mathbf{E} = (E_x, E_y, E_z)$ is the electric field vector, and T represents the transpose of the vector. In the following text, the vector or tensor is represented by bold symbol.

In an arbitrary coordinate system σ - xyz (Fig. 1a), the conductivity tensor can be expressed, in terms of components, as follows:

$$J_i = \sum_j^{x,y,z} \sigma_{ij}E_j, \quad i = x, y, z, \tag{2}$$

where σ_{ij} represents the components of the conductivity tensor, which can be written as:

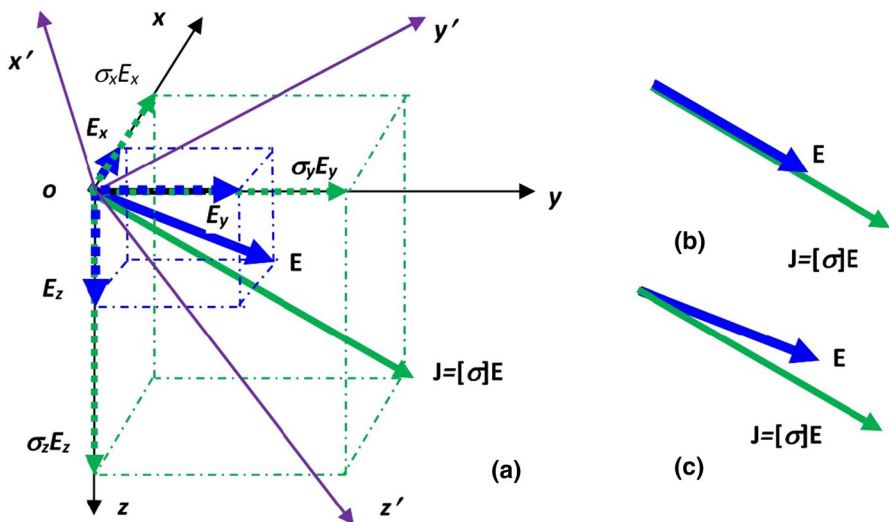


Fig. 1 Components of current density when a field is applied. The relation between the electric current density \mathbf{J} and the electric field \mathbf{E} in **b** isotropic media and **c** anisotropic media. The thin black arrows are original coordinate system σ - xyz while the thin purple arrows are new coordinate system σ - $x'y'z'$. See text in Sect. 2 for the meaning of symbols

$$\boldsymbol{\sigma} = [\sigma_{ij}] = \begin{bmatrix} \sigma_{xx} & \sigma_{xy} & \sigma_{xz} \\ \sigma_{yx} & \sigma_{yy} & \sigma_{yz} \\ \sigma_{zx} & \sigma_{zy} & \sigma_{zz} \end{bmatrix}. \tag{3}$$

In an isotropic medium, the direction of the electric field is parallel to that of the current density, and thus, $\boldsymbol{\sigma}$ becomes a scalar σ (Fig. 1b). In such case, we have

$$j_x = \sigma E_x, j_y = \sigma E_y, j_z = \sigma E_z, \tag{4}$$

where j_x, j_y and j_z are the components of current density in x, y, z directions, respectively, and correspondingly, the E_x, E_y and E_z are the components of electric field.

In an anisotropic medium, the direction of the electric field is different than that of the current density (Fig. 1c). In this case, from Eqs. (1)–(3), we obtain the following expressions which relate the current density components and the electric field components by the conductivity tensor components (Fig. 1a):

$$j_x = \sigma_{xx}E_x + \sigma_{xy}E_y + \sigma_{xz}E_z, \tag{5}$$

$$j_y = \sigma_{yx}E_x + \sigma_{yy}E_y + \sigma_{yz}E_z, \tag{6}$$

$$j_z = \sigma_{zx}E_x + \sigma_{zy}E_y + \sigma_{zz}E_z. \tag{7}$$

In the geo-electromagnetics, the Hall conductivity, the Cowling conductivity and the Pedersen conductivity as well as the dispersion effect are generally not considered; hence, the anisotropic conductivity tensor may be regarded to be symmetric positive definite.

3 The Conductivity Tensor Under the Rotation of the Coordinate System

Discussions of the rotation of the conductivity (or resistivity) tensor are given in many MT studies (Pek and Verner 1997; Heise et al. 2006; Pek and Santos 2006; Miensopust and Jones 2011; Mandolesi 2013; Martí 2014), in which the rotation of the conductivity tensor is carried out by applying three successive Euler rotations. Here is another more general description about the conductivity tensor under the rotation of the coordinate system.

Assuming that the original coordinate system $o-xyz$ is rotated into the new coordinate system $o-x'y'z'$ (Fig. 1a), the electric field in the new coordinate system can be expressed as (Nye 1985):

$$\mathbf{E}' = \mathbf{R}\mathbf{E}, \tag{8}$$

where

$$\mathbf{R} = \begin{bmatrix} \alpha_{x'x} & \alpha_{x'y} & \alpha_{x'z} \\ \alpha_{y'x} & \alpha_{y'y} & \alpha_{y'z} \\ \alpha_{z'x} & \alpha_{z'y} & \alpha_{z'z} \end{bmatrix} \tag{9}$$

is the rotation matrix and α_{ij} ($i = x', y', z'; j = x, y, z$) represents the cosine of the angle between the i - and j -axis.

The electric field in the original coordinate system can be expressed in terms of the one in the new coordinate system via the following expression:

$$\mathbf{E} = \mathbf{R}^{-1}\mathbf{E}' = \mathbf{R}^T\mathbf{E}', \tag{10}$$

where \mathbf{R}^T is the transpose matrix of \mathbf{R} .

The conductivity tensor in the new coordinate system can be written as:

$$\bar{\sigma} = \mathbf{R}\sigma\mathbf{R}^T \tag{11}$$

where $\bar{\sigma}$ is the representation of σ in the new coordinate system $o-xyz$.

4 Ellipsoid Representation of the Conductivity Tensor

Generally, $\sigma = [\sigma_{ij}]$ is a symmetric second-rank tensor for crystals; the proof is referred to Feynman et al. (1965). This conclusion also holds for the general Earth medium. Therefore, for a general Earth medium, according to Eqs. (1)–(3), the dissipated energy flow density per unit volume can be written as:

$$U_p = \frac{1}{2}\mathbf{E} \cdot \mathbf{j} = \frac{1}{2}\mathbf{E} \cdot \sigma\mathbf{E}^T = \frac{1}{2} \sum_i \sum_j \sigma_{ij}E_iE_j, \quad i, j = x, y, z. \tag{12}$$

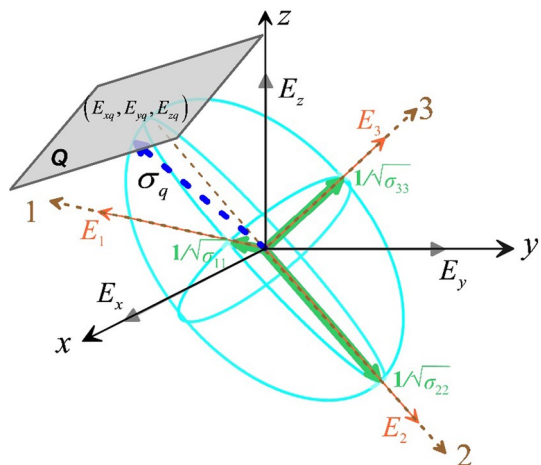
For a given power flow $U_0/2$, Eq. (12) can be expanded as:

$$\sigma_{xx}E_x^2 + \sigma_{yy}E_y^2 + \sigma_{zz}E_z^2 + 2\sigma_{xy}E_xE_y + 2\sigma_{yz}E_yE_z + 2\sigma_{zx}E_zE_x = U_0 \tag{13}$$

Equation (13) represents an ellipsoid which is the trajectory of a vector $\mathbf{E} = (E_x, E_y, E_z)$ with a constant energy, and is called as an energy ellipsoid. The normal direction at any point q on the tangent plane Q of the energy ellipsoid is $\mathbf{E}_q = (E_{xq}, E_{yq}, E_{zq})$ (the vector shown by the dashed blue arrow in Fig. 2).

According to the mathematical representation of the quadratic function, there always exists such a coordinate system in which only the diagonal elements of the conductivity tensor

Fig. 2 Energy ellipsoid—the trajectory of the vector $E=(E_x, E_y, E_z)$ with constant energy. The coordinate axes 1, 2 and 3 are taken to be the anisotropic principal axes and represented in brown dashed lines. The orange solid arrows marked as E_1, E_2 and E_3 are equivalent to the principal axes 1, 2, 3. The three semi-axes of the ellipsoid are represented by green solid arrows with lengths $1/\sqrt{\sigma_{11}}$, $1/\sqrt{\sigma_{22}}$ and $1/\sqrt{\sigma_{33}}$. The thick dashed arrow in blue is the conductivity vector at the point q at the surface of the ellipsoid



exist while off-diagonal elements vanish. The three coordinate axes in such coordinate system are called as the principal axes, denoted by 1-, 2- and 3-axis (as indicated by the axis in brown dashed line in Figs. 2 and 3). In this coordinate system, σ_{ij} attains extreme values (i.e., the three principal values of the conductivity tensor σ_{11} , σ_{22} and σ_{33}), and then on the corresponding tangent planes, off-diagonal elements of the conductivity tensor vanish, that is, $\sigma_{xy} = \sigma_{yz} = \sigma_{zx} = 0$. And hence, we obtain a normalized equation for the ellipsoid as follows:

$$\sigma_{11}E_1^2 + \sigma_{22}E_2^2 + \sigma_{33}E_3^2 = 1 \tag{14}$$

where E_1 , E_2 and E_3 are the new principal axes which are equivalent to the principal axes 1, 2 and 3, respectively. For the sake of consistency, these principal axes are uniformly represented by axes 1, 2 and 3 (as indicated by the axis in brown dashed line in Figs. 2 and 3), respectively. Therefore, for these three axes, there are only three nonzero components in the conductivity tensor. The lengths of the three semi-axes of the ellipsoid are $1/\sqrt{\sigma_{11}}$, $1/\sqrt{\sigma_{22}}$ and $1/\sqrt{\sigma_{33}}$, respectively. When a unit electric field vector is considered in Eq. (12), Eq. (13) can be rewritten as:

$$\sigma_{xx}l_x^2 + \sigma_{yy}l_y^2 + \sigma_{zz}l_z^2 + 2\sigma_{xy}l_xl_y + 2\sigma_{yz}l_yl_z + 2\sigma_{zx}l_zl_x = \sigma_q, \tag{15}$$

where $\mathbf{e} = (l_x, l_y, l_z)$ represents the unit vector in the direction of the electric field and σ_q is the conductivity in the normal direction of the point q on the tangent plane Q , or in the direction of the electric field \mathbf{E}_q (as shown in the blue arrow in Fig. 2). $l_x = E_x/E, l_y = E_y/E$ and $l_z = E_z/E$ indicate the direction cosine of the electric field \mathbf{E} . If the conductivity at the point q in space is regarded as the vector, then the amplitude of the conductivity vector at this point is $\sigma_q = \sqrt{\sigma_{qx}^2 + \sigma_{qy}^2 + \sigma_{qz}^2}$ and $\mathbf{e}_q = (l_{qx}, l_{qy}, l_{qz})$, respectively. Hence, we can obtain that $l_{qx} = \sigma_{qx}/\sqrt{\sigma_q}$, $l_{qy} = \sigma_{qy}/\sqrt{\sigma_q}$ and $l_{qz} = \sigma_{qz}/\sqrt{\sigma_q}$. σ_{qx} , σ_{qy} and σ_{qz} are the components of the conductivity vector at the point q in axes x, y, z , respectively. Substituting l_{qx}, l_{qy} and l_{qz} into Eq. (15), one can obtain

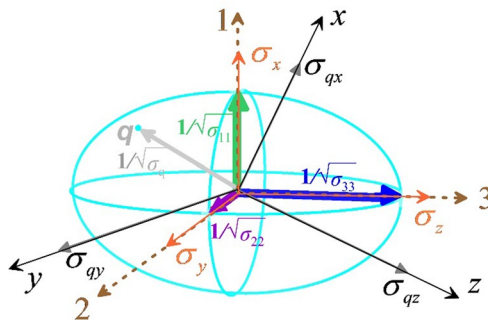


Fig. 3 Conductivity ellipsoid in the principal coordinate system 123. The coordinate axes 1, 2 and 3 are taken to be the anisotropic principal axes and represented in brown dashed lines. The orange solid arrows marked as σ_x , σ_y and σ_z are equivalent to the principal axes 1, 2, 3. The three semi-axes of the ellipsoid are indicated by solid arrow in green, purple and blue, respectively, and their lengths are $1/\sqrt{\sigma_{11}}$, $1/\sqrt{\sigma_{22}}$ and $1/\sqrt{\sigma_{33}}$. The thick solid arrow in gray is the conductivity vector at the point q at the surface of the ellipsoid. The thin solid arrows labeled with σ_{qx}, σ_{qy} and σ_{qz} are the components of the conductivity vector at the point q in any arbitrary coordinate system with axes x, y, z represented by black solid arrows. See the texts following Eq. (15–17) in Sect. 4 for details

$$\sigma_{xx}\sigma_{qx}^2 + \sigma_{yy}\sigma_{qy}^2 + \sigma_{zz}\sigma_{qz}^2 + 2\sigma_{xy}\sigma_{qx}\sigma_{qy} + 2\sigma_{yz}\sigma_{qy}\sigma_{qz} + 2\sigma_{zx}\sigma_{qz}\sigma_{qx} = 1. \tag{16}$$

Obviously, Eq. (16) represents the equation of the ellipsoid. Therefore, if the coordinate axes are taken to be parallel to the directions of σ_{qx} , σ_{qy} and σ_{qz} , then the ellipsoid represented by Eqs. (15) or (16) is also called conductivity tensor ellipsoid (as shown in Fig. 3). If the coordinate axes are taken to be the principal axes 1, 2 and 3, then Eq. (16) can be rewritten as:

$$\sigma_{11}\sigma_x^2 + \sigma_{22}\sigma_y^2 + \sigma_{33}\sigma_z^2 = 1. \tag{17}$$

Similar to Eq. (14), it can be seen from Eq. (17) that σ_x , σ_y and σ_z can be considered as the new principal axes. And they are equivalent to the principal axes 1, 2 and 3. Hence, the lengths of the three semi-axes of the ellipsoid are also $1/\sqrt{\sigma_{11}}$, $1/\sqrt{\sigma_{22}}$ and $1/\sqrt{\sigma_{33}}$, as shown in Fig. 3.

The problem of finding the principal conductivities is equivalent to finding the eigenvalues and eigenvectors of the following equation (Nye 1985):

$$(\boldsymbol{\sigma} - \lambda\mathbf{I})\mathbf{e} = 0, \tag{18}$$

where \mathbf{I} is unit matrix.

The three eigenvalues of Eq. (18) are the roots of the following characteristic polynomial equation:

$$\det(\boldsymbol{\sigma} - \lambda\mathbf{I}) = \lambda^3 + C_1\lambda^2 + C_2\lambda + C_3 = 0, \tag{19}$$

where

$$C_1 = -(\sigma_{xx} + \sigma_{yy} + \sigma_{zz}), \tag{20}$$

$$C_2 = \sigma_{xx}\sigma_{yy} + \sigma_{yy}\sigma_{zz} + \sigma_{zz}\sigma_{xx} - \sigma_{xy}^2 - \sigma_{yz}^2 - \sigma_{zx}^2, \tag{21}$$

$$C_3 = \sigma_{xx}\sigma_{yz}^2 + \sigma_{yy}\sigma_{zx}^2 + \sigma_{zz}\sigma_{xy}^2 - \sigma_{xx}\sigma_{yy}\sigma_{zz} - 2\sigma_{xy}\sigma_{yz}\sigma_{zx} \tag{22}$$

The coefficients C_1 , C_2 and C_3 in Eq. (19) are invariants when the axes are rotated, which can be shown by solving Eq. (19) for three roots σ_{11} , σ_{22} and σ_{33} :

$$C_1 = -(\sigma_{11} + \sigma_{22} + \sigma_{33}), \tag{23}$$

$$C_2 = \sigma_{11}\sigma_{22} + \sigma_{22}\sigma_{33} + \sigma_{33}\sigma_{11}, \tag{24}$$

$$C_3 = \sigma_{11}\sigma_{22}\sigma_{33}. \tag{25}$$

Substituting σ_{11} , σ_{22} and σ_{33} into Eq. (18), the corresponding principal axes \mathbf{e}_1 , \mathbf{e}_2 and \mathbf{e}_3 , which represent the unit vector along the directions of the principal axes, can be found.

Obviously, the difference $(\sigma_{11} - \sigma_{33})$ between the maximum and minimum principal conductivities reflects the strength of anisotropy. The flatness ($\alpha = (\sqrt{\sigma_{11}} - \sqrt{\sigma_{33}})/\sqrt{\sigma_{11}}$) or ellipticity ($\beta = \sqrt{\sigma_{11}/\sigma_{33}}$) of the conductivity tensor ellipsoid can be used to indicate the strength of the anisotropy.

5 The Representation of the Conductivity Tensor with Mohr Circle

Mohr circle was first proposed to represent stress by German civil engineer Culmann (1866) and extended in detail by German civil engineer Mohr (1882). Mohr circle is one of the few graphical techniques still used in stresses tensor analysis. It provides a simple and clear picture of an otherwise complicated analysis (Ferdinand and Johnson 1992).

Mohr circles were introduced in geophysics to relate shear stress and normal stress (Jaeger 1969) and used to represent tensor information as a general application (Nye 1985); Mohr circles were first introduced by Lilley (1976) into magnetotellurics to represent magnetotelluric impedance tensors. Hereafter, Lilley (1993a) further explored the application of Mohr circle in the display of magnetotelluric data and used the Mohr circles in magnetotelluric data interpretation when static shift occurs (Lilley 1993b). In addition, the Mohr circle is also used to perform MT tensor decomposition and galvanic distortion analysis (Lilley 1998b, 1998a, 2012). Moreover, Mohr circles were used to identify regional dimensionality and strike angle from distorted magnetotelluric data (Weaver 2004; Weaver and Lilley 2004; Lilley 2016, 2018). However, reports of the use of Mohr circles for conductivity tensors have not yet appeared. Therefore, a graphical representation of the Mohr circle of the conductivity tensor is presented here.

We first consider the Mohr circle for the 2-D case defined by x and y coordinates; in this case the conductivity tensor can be written as

$$\sigma = \begin{bmatrix} \sigma_{xx} & \sigma_{xy} \\ \sigma_{yx} & \sigma_{yy} \end{bmatrix}$$

in the arbitrary coordinate systems. In the anisotropic principal coordinate system defined by axes 1 and 2, it can be expressed as

$$\sigma = \begin{bmatrix} \sigma_{11} & 0 \\ 0 & \sigma_{22} \end{bmatrix}.$$

The corresponding Mohr circle is shown in Fig. 4. Similar to the stresses tensor analysis (Ugural and Fenster 2011), in 2-D space, the coordinate of the center of the Mohr circle on the horizontal axis is

$$oO_1 = (\sigma_{11} + \sigma_{22})/2, \tag{26}$$

and its radius is

$$r = (\sigma_{11} - \sigma_{22})/2, \tag{27}$$

where $\sigma_{11} > \sigma_{22}$.

The abscissa of a point on the Mohr circle

$$\sigma_n(\theta) = \sigma_{ii}(\theta) = oO_1 + r\cos 2\theta, \quad i = 1, 2, \tag{28}$$

indicates the diagonal components of the conductivity tensor, where 2θ is the rotation angle of the coordinate axis with respect to the principal axis. $\sigma_n(\theta)$ takes the maximum value σ_{11} when $\theta = 0^\circ$, while it takes the minimum value σ_{22} when $\theta = 90^\circ$.

The ordinate of a point on the Mohr circle

$$\sigma_{ij}(\theta) = r\sin 2\theta, \quad (i \neq j; i, j = 1, 2) \tag{29}$$

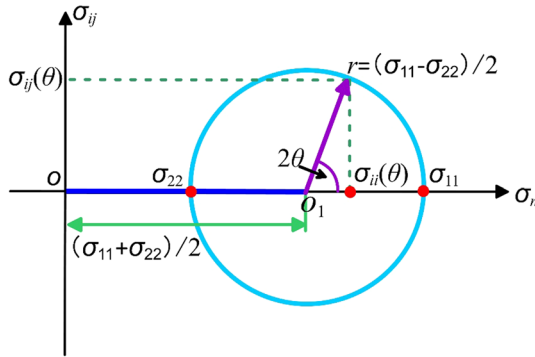


Fig. 4 Graphical representation for the 2-D tensor identical conductivity state by using Mohr circle of conductivity tensor in rotated principal axis coordinate system. The abscissa axis is related to the diagonal elements of the conductivity tensor $\sigma_n = \sigma_{ij}$ ($i = j = 1, 2$), while the ordinate axis is taken as the off-diagonal elements of the conductivity tensor $\sigma_{ij} = (\sigma_{ii} - \sigma_{jj})/2$ ($i \neq j; i, j = 1, 2$). The abscissa at the center (O_1) of the circle is equal to the average principal conductivities $(\sigma_{11} + \sigma_{22})/2$. The maximum σ_{11} and minimum σ_{22} conductivities define the diameter in the principal frame ($\theta = 0$). Any other point on the circle gives the conductivity tensor in a coordinate system rotated by 2θ from the principal axis. The red points marked with σ_{11} and σ_{22} are the point of intersection of the Mohr circle and the abscissa axis. The red point labeled by $\sigma_{ii}(\theta)$ represents the abscissa of the point corresponding to angle θ on the Mohr circle. $\sigma_{ij}(\theta)$ represents the ordinate the point corresponding to angle θ on the Mohr circle

indicates the off-diagonal components of the conductivity tensor. Obviously it relates to the difference in conductivities along different principal directions, which is due to the conductivity anisotropy. σ_{ij} takes the maximum value $(\sigma_{11} - \sigma_{22})/2$ when $\theta = 45^\circ$.

It can be seen from Fig. 4 and equation

$$\sigma_{ij}(\theta) = r \sin 2\theta = (\sigma_{11} - \sigma_{22}) \sin 2\theta / 2 \quad (i \neq j; i, j = 1, 2) \tag{29'}$$

that the magnitude of off-diagonal elements is a measure of electrical anisotropy. The magnitude of the off-diagonal elements varies with the coordinate rotation and is equal to the ordinate of the point on the Mohr circle. The abscissa of some point on the Mohr circle takes the maximum value σ_{11} and the minimum value σ_{22} , respectively, on the principal axis $\theta = 0$. When the conductivities along the two principal directions are equal to each other (i.e., $\sigma_{11} = \sigma_{22}$), the Mohr circle degenerates into a point. Therefore, the size of Mohr circle is the measure of the strength of the electrical anisotropy, and the Mohr circle provides a visual description of the variation in the elements of the conductivity tensor along the axes. It should be noted that the Mohr circle was drawn in the coordinate system defined by the σ_n and σ_{ij} rather than in the o - xyz coordinate system.

In the 3-D case defined by the x , y and z coordinates, when drawing a Mohr circle, only two of the three coordinates x , y and z are considered at a time, and the 3-D case can be considered as three 2-D situations (i.e., xy , yz and zx). It is also noted that the Mohr circle will be not drawn in the o - xyz coordinate system but in the coordinate system defined by the σ_n and σ_{ij} as in 2-D case. The drawing of the Mohr circle in each situation is completely similar to the 2-D case. If $\sigma_{ij} = (\sigma_{ii} - \sigma_{jj})/2$ ($i \neq j; i, j = 1, 2, 3$) is taken as the ordinate axis and $\sigma_n = \sigma_{ij}$ ($i = j = 1, 2, 3$) is taken as the abscissa axis, one can draw the 2-D Mohr circles in these three combinations on the same plane. If the problem is considered in the principal coordinate system and conductivities along the three principal axes (1, 2 and 3)

are sorted from large to small (i.e., $\sigma_{11} \geq \sigma_{22} \geq \sigma_{33}$), then the differences in conductivities along two of the three principal axes can be defined as the radii of the Mohr circle:

$$\sigma_{23} = (\sigma_{22} - \sigma_{33})/2, \tag{30}$$

$$\sigma_{13} = (\sigma_{11} - \sigma_{33})/2, \tag{31}$$

$$\sigma_{12} = (\sigma_{11} - \sigma_{22})/2, \tag{32}$$

where σ_{12} , σ_{13} and σ_{23} are half of the differences in conductivities between the principal axes 1 and 2, 1 and 3, as well as 2 and 3, respectively.

The coordinates of the centers of the Mohr circle on the horizontal axis are:

$$oO_3 = (\sigma_{22} + \sigma_{33})/2, \tag{33}$$

$$oO_2 = (\sigma_{22} + \sigma_{11})/2, \tag{34}$$

$$oO_1 = (\sigma_{11} + \sigma_{33})/2. \tag{35}$$

According to Eqs. (30)–(35), three Mohr circles for 3-D case can be drawn (Fig. 5).

It is clear from Eqs. (30)–(32) that the relationship between the maximum principal conductivities satisfies

$$\sigma_{11} = \sigma_{33} + 2\sigma_{12} + 2\sigma_{23}, \tag{36}$$

which means that the conductivity σ_{11} in the principal direction 1 can be represented into the combination of the conductivity σ_{33} in the principal direction 3 with σ_{12} and σ_{13} .

Similarly, from Eqs. (31) and (36), one obtains

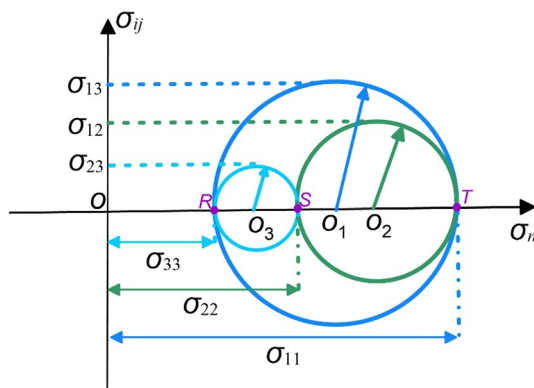


Fig. 5 Mohr circles for 3-D tensor with identical conductivity state. The abscissa axis is related to the diagonal elements of the conductivity tensor $\sigma_n = \sigma_{ij} (i = j = 1, 2, 3)$, while the ordinate axis is taken as the off-diagonal elements of the conductivity tensor $\sigma_{ij} = (\sigma_{ii} - \sigma_{jj})/2 (i \neq j; i, j = 1, 2, 3)$. σ_{11} , σ_{22} and $\sigma_{33} (\sigma_{11} \geq \sigma_{22} \geq \sigma_{33})$ are the conductivities along the three principal axes. σ_{12} , σ_{13} and σ_{23} are half of the differences between the principal conductivities. The purple points R , S and T represent the intersections of three Mohr circles and the abscissa axis

$$\sigma_{13} = \sigma_{12} + \sigma_{23} \quad (37)$$

by which σ_{13} can be expressed as the sum of σ_{12} and σ_{23} . Equations (36) and (37) establish some connections between quantities such as σ_{11} , σ_{12} , σ_{13} , σ_{23} and σ_{33} , which facilitates checking whether they are correctly obtained, as shown in Fig. 5.

The axis of ordinates is taken as

$$\sigma_{ij} = \sigma_{ii} - \sigma_{jj}, i \neq j; i, j = 1, 2, 3, \quad (38)$$

and the axis of abscissas is taken as

$$\sigma_n = \sigma_{ij}, i = j = 1, 2, 3. \quad (39)$$

Then, the Mohr circle representation of the conductivity tensor in 3-D case can be drawn as shown in Fig. 5.

The pattern distribution of Mohr circle can visually indicate the conductivity along each principal direction. The radius of each Mohr circle reflects the difference in conductivities along the anisotropy principal axes. The relative position distribution of Mohr circle can graphically display the difference in conductivities along each principal direction.

The Mohr circle representation of the stress tensor has been widely used in the fields of seismology and engineering. In particular, the Mohr circle can be used to easily find the maximum and minimum stresses and their ratios, to study stress and strain changes in the Earth (Sarma 1975), fluid pressure in rock jointing (Secor 1965; McKeagney et al. 2004) and in rock rupture (Griffiths 1990; Jolly and Sanderson 1997; Labuz and Zang 2012), thus playing an important role in these applications. Compared to anisotropic seismic wave (P or S wave) velocity tensors in the Earth, the difference between the magnitudes of the three principal elements in the anisotropic conductivity tensor may be several orders of magnitude greater. In seismology, the seismic wave velocity can be linked to the stress and strain by Hooke's law, so as to achieve the purpose of studying the geo-stress. This suggests that there are some advantages in studying the anisotropy of the Earth's medium using conductivity tensors compared with seismic wave velocity tensors. This advantage can be manifested by the Mohr circle representation of the conductivity tensor, a similar representation of the Mohr circle of the geo-stress tensor.

Unlike the ellipsoid representation of the conductivity tensor, the Mohr circle representation of the conductivity tensor can conveniently show the values of the elements of the conductivity tensor in arbitrary directions. As the maximum and minimum stresses and their ratios can be calculated by Mohr circle from the stress in arbitrary direction, the maximum and minimum conductivity and their ratio can be determined more conveniently using the Mohr circle from the conductivity tensor in arbitrary direction, which is also more convenient than the ellipsoid representation of the conductivity tensor. The Mohr circle representation also provides a more convenient tool for mutual reference and comparison so as to carry out a joint study of conductivity tensor and stress tensor.

A possible reason that there has been no previous practical application of Mohr circles in geo-electromagnetics is that it is difficult to completely reconstruct all components of the conductivity tensor for anisotropic media in arbitrary coordinate system, although it is possible to reconstruct a conductivity tensor in a specified coordinate system based on particular physical models for a very long time. This fact could be also a possible reason why the representations of the conductivity tensor by Mohr circles have not received much attention so far. However, the authors believe that with the development of the forward and

inversion techniques for generally anisotropic conductivity tensor, Mohr circles of the conductivity tensor should also have some favorable application prospects.

From the above text, one can get some general information about how Mohr circles are constructed and what they represent, e.g., that:

1. They provide a graphic representation of a tensor as a function of the rotation of the coordinate system. The circle is the locus of points representing the form of the tensor on individual planes at all their orientations, where the axes represent the principal axes of the tensor.
2. For a 2-D system, the single Mohr circle plots σ_{ij} versus σ_n as the coordinate system rotates through 180° . The plot is based on the principal components of the tensor: The limits on the horizontal axis relate to the principal values of the tensor, and the limits on vertical axis relate to the difference between principal values.
3. For a 3-D system, the three possible Mohr circles corresponding to pairs of principal values and the abscissa and ordinate of each point on the circle are again the magnitudes of the diagonal component and off-diagonal components, respectively, as axes are rotated in each of the planes $\sigma_{12}\sigma_n$, $\sigma_{23}\sigma_n$, $\sigma_{31}\sigma_n$.

6 Geometric form Representation of the Conductivity Tensor Model and Its Explanation

The actual electrical anisotropic Earth may correspond to various conductivity models which can be expressed in different forms of tensors. There are many publications describing how various geometric forms to contribute to anisotropic conductivity including for films, rods, resistor networks, embedded ellipsoids (Grant and West 1965; Madden 1976; Schmeling 1986; Bigalke 1999, 2000a, b; Kozlovskaya and Hjelt 2000; Bahr et al. 2002; Pervukhina et al. 2005; Wannamaker 2005; Pommier 2014; Kirkby and Heinson 2015; Schön 2015; Kirkby et al. 2016a, b; Kirkby and Heinson 2017).

Many substances consist of anisotropic conductive crystal unit cells, which are formed by oriented small particles of different compositions and/or small blocks with aligned fractures. The electrical anisotropy characteristic usually exhibited by these crystal unit cells is called electrical microscopic anisotropy. On the other hand, the repeated recurrence of the alignment of the cells of these anisotropic crystal units results in so-called electrical macroscopic anisotropy (Maillet 1947; Eisel and Haak 1999).

The anisotropic conductivity tensor can be considered as representing some geometric combination of homogeneous isotropic prisms with different conductivities. These conductivity geometric models are mainly divided into four categories in the principal coordinate system, which will be discussed in detail below.

6.1 Case 1: Uniaxial Anisotropy with Infinitely Repeated HTI/VTI Unit

In all possible electrical conductivity tensors in the principal coordinate system, the uniaxial anisotropic tensor (that is, the electrical conductivity tensor with a principal component different from the other two) is the simplest case. In this case, the conductivity structures can be represented by geometric forms as shown in Fig. 6, which can also be considered as horizontal transverse isotropy (HTI) (Fig. 6a) or vertical transverse isotropy (VTI) (Fig. 6b and c). If the problem is considered in the principal coordinate

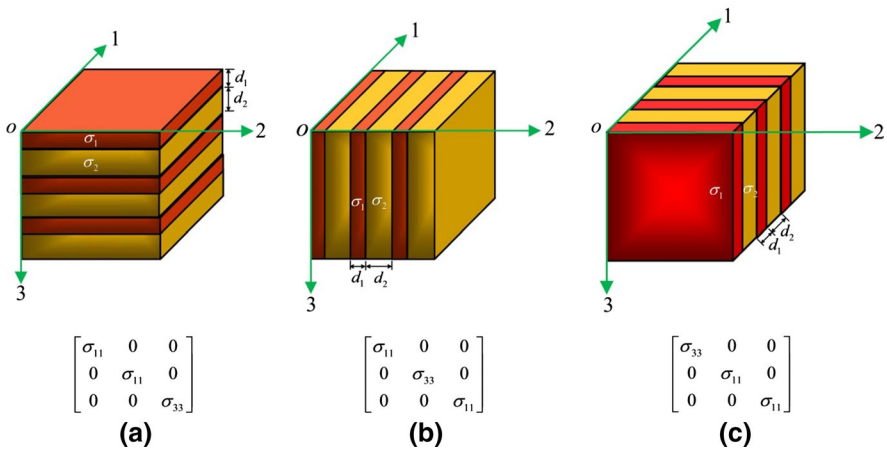


Fig. 6 Geometric graph representation of the uniaxial anisotropic conductivity tensor (case 1) given by Eqs. (40a–c) and (41–42) in the principal axis coordinate system. The model **a** can be considered as HTI, and models **b** and **c** are VTI structures. The corresponding conductivity tensors are given in the panel below each graph. The graphs in **b** and **c** can be considered as the ones obtained when the graph **a** is rotated 90° around the *x*- and *y*-axis, respectively

system in which the principal axes are denoted by 1, 2 and 3 axes, and $\sigma_{11} = \sigma_{22} \neq \sigma_{33}$, then the conductivity tensor can be written as:

$$\sigma' = \begin{bmatrix} \sigma_{11} & 0 & 0 \\ 0 & \sigma_{11} & 0 \\ 0 & 0 & \sigma_{33} \end{bmatrix}, \tag{40a}$$

$$\sigma'' = \begin{bmatrix} \sigma_{11} & 0 & 0 \\ 0 & \sigma_{33} & 0 \\ 0 & 0 & \sigma_{11} \end{bmatrix}, \tag{40b}$$

$$\sigma''' = \begin{bmatrix} \sigma_{33} & 0 & 0 \\ 0 & \sigma_{11} & 0 \\ 0 & 0 & \sigma_{11} \end{bmatrix}, \tag{40c}$$

which correspond to the subfigures as shown in Fig. 6a–c, respectively. The model shown in Fig. 6a can be considered to be a stack of thin layers composed of two different media, in which two adjacent layers have different compositions and same thickness, and all the layers are parallel to the *xoy* plane. The thickness and conductivity of the first medium (the layer in red in Fig. 6a–c) are d_1 and σ_1 , respectively. The thickness and conductivity of the second medium (the layer in yellow in Fig. 6a–c) are d_2 and σ_2 , respectively. Therefore, according to Ohm’s law, the macroscopic equivalent conductivity in the 1 (parallel and series association of resistances) and 3 directions (series association of resistances) can be derived as:

$$\sigma_{11} = \frac{(d_1\sigma_1 + d_2\sigma_2)}{d_1 + d_2}, \quad (\text{parallel}) \tag{41}$$

$$\sigma_{33} = \frac{d_1 + d_2}{d_1/\sigma_1 + d_2/\sigma_2}. \quad (\text{series}) \tag{42}$$

The models (b) and (c) in Fig. 5 can be considered as the ones obtained when the model (a) is rotated 90° around the 1- and 2-axis, respectively. Therefore, the macroscopic equivalent conductivity can also be calculated using Eqs. (41) and (42).

Many others authors (Maillet 1947; Eisel and Haak 1999; Mollison et al. 1999; Schön et al. 1999; Schön et al. 2000; Schön 2015; Wiese et al. 2015) also gave the same, or similar equation as Eqs. (41) and (42).

Obviously, if $\sigma_1 = \sigma_2$, Eqs. (41) and (42) reduce to the isotropic case (i.e., $\sigma_{11} = \sigma_{33} = \sigma_1$).

6.2 Case 2: Simply Biaxial Anisotropy with Infinitely Repeated HTI/VTI Unit

Another form of anisotropic electrical conductivity is biaxial anisotropic conductivity (Mogilatov and Bespalov 2009; Yuan et al. 2010; Davydycheva and Wang 2011), also known as triaxial anisotropic conductivity in some literature (Nekut 1994; Yu et al. 1997; Hoversten et al. 2015). It is characterized by three different conductivity values along each of the three different principal axes. In this section, we consider a model consists of an array of infinitely long rectangular prisms with alternating conductivity resulting in a conductivity structure that varies along axes perpendicular to the rods but is invariant in the direction parallel to the prisms. This graphical representation of the biaxial anisotropic conductivity tensor can be illustrated in a form of the geometric models with infinitely repeated HTI (Fig. 7a) or VTI unit (Fig. 7b and c) unit.

When $\sigma_{11} \neq \sigma_{22} \neq \sigma_{33}$, the conductivity tensor in the principal axis coordinates system can be expressed as:

$$\sigma' = \begin{bmatrix} \sigma_{11} & 0 & 0 \\ 0 & \sigma_{22} & 0 \\ 0 & 0 & \sigma_{33} \end{bmatrix}, \tag{43a}$$

$$\sigma'' = \begin{bmatrix} \sigma_{11} & 0 & 0 \\ 0 & \sigma_{33} & 0 \\ 0 & 0 & \sigma_{22} \end{bmatrix}, \tag{43b}$$

$$\sigma''' = \begin{bmatrix} \sigma_{33} & 0 & 0 \\ 0 & \sigma_{22} & 0 \\ 0 & 0 & \sigma_{11} \end{bmatrix}, \tag{43c}$$

which can be represented by the models shown in Fig. 7a, c, d, respectively.

Similar to case 1, the models shown in Fig. 7 are formed by two sets of rectangular prisms with different conductivities and dimensions, which are arranged alternately side

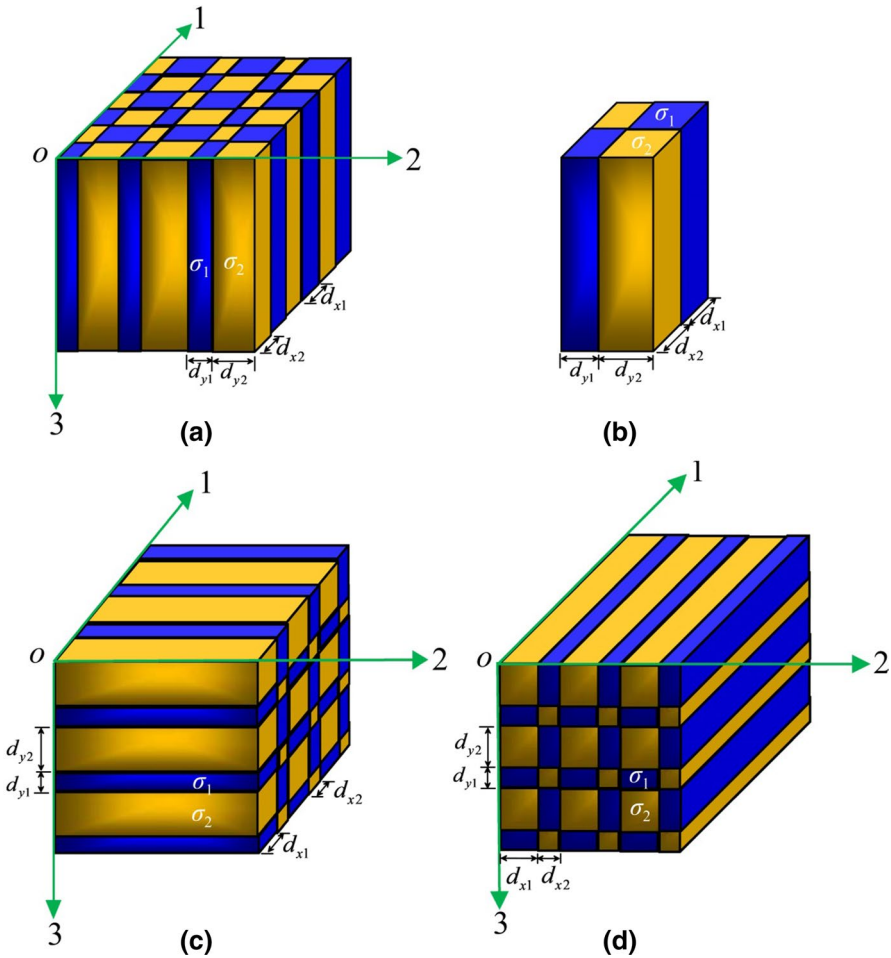


Fig. 7 Geometric graph representation of the simply biaxial anisotropic conductivity tensor (case 2) given by Eqs. (43a–c) and (44a–c) in the principal axis coordinate system. The model **a** can be considered as infinitely repeated VTI, and models **c** and **d** are infinitely repeated HTI. The graph in panel **a** is constructed by alternately arranging many sets of rectangular prisms with different conductivities and dimensions side by side. Each set of prisms consists of four cubes shown in panel **(b)**. The geometric graphs shown in subfigure **c** and **d** can be regarded as the ones obtained when the geometric graph **a** is rotated 90° around the *x*- and *y*-axis, respectively

by side. Each set of prisms infinitely extends along the 1-, 2-, 3-axis. Take the model shown in Fig. 7a as an example; the blue rectangular prism has the dimension of d_{x1} and d_{y1} in the direction of the 1- and 2-axis, respectively. The yellow rectangular prism has the dimension of d_{x2} and d_{y2} in the direction of the 1- and 2-axis, respectively. The conductivities of the blue rectangular prism and the yellow one are σ_1 and σ_2 , respectively. This model (Fig. 7a) can be regarded as cyclic repetition of the combination of four adjacent prisms shown in Fig. 7b. Therefore, the equivalent conductivity of this model can be obtained by calculating the total conductivity of the combined prisms shown in

Fig. 7b. From Ohm’s law, the macroscopic equivalent conductivities along three principal directions can be derived as:

$$\sigma_{11} = \frac{\sigma_1\sigma_2(d_{x1} + d_{x2})}{(d_{y1} + d_{y2})} \left[\frac{d_{y1}}{(\sigma_2d_{x1} + \sigma_1d_{x2})} + \frac{d_{y2}}{(\sigma_1d_{x1} + \sigma_2d_{x2})} \right] \tag{44a}$$

$$\sigma_{22} = \frac{\sigma_1\sigma_2(d_{y1} + d_{y2})}{(d_{x1} + d_{x2})} \left[\frac{d_{x1}}{(\sigma_2d_{y1} + \sigma_1d_{y2})} + \frac{d_{x2}}{(\sigma_1d_{y1} + \sigma_2d_{y2})} \right] \tag{44b}$$

$$\bar{\sigma}_{33} = \frac{d_{y1}(\sigma_1d_{x1} + \sigma_2d_{x2}) + d_{y2}(\sigma_1d_{x2} + \sigma_2d_{x1})}{(d_{x1} + d_{x2})(d_{y1} + d_{y2})}. \tag{44c}$$

The models shown in Fig. 7c, d can be considered as the ones obtained when the model in Fig. 7a is rotated 90° around the 1- and 2-axis, respectively. Therefore, the macroscopic equivalent conductivity for these models can be calculated by substituting Eqs. (44a–c) into Eqs. (43a–c).

6.3 Case 3: More General Biaxial Anisotropy with Infinitely Repeated HTI/VTI Unit

Similar to the last case, in this section we consider a biaxial anisotropic conductivity tensor with more general infinitely repeated horizontal (Fig. 8a) or vertical (Fig. 8b, c) transverse isotropy. In this model, the values of the conductivity of the alternating prisms differ along the two axes perpendicular to the prisms.

Similar to case 3, four adjacent prisms shown in Fig. 8b have different dimensions and conductivity. The red rectangular prism has the dimension of d_{x1} and d_{y1} in the direction of the 1- and 2-axis, respectively, and its conductivity is σ_1 . The yellow rectangular prism has the dimension of d_{x1} and d_{y2} in the direction of the 1- and 2-axis, respectively, and its conductivity is σ_2 . The blue rectangular prism has the dimension of d_{x2} and d_{y2} in the direction of the 1- and 2-axis, respectively, and its conductivity is σ_3 . The green rectangular prism has the dimension of d_{x2} and d_{y1} in the direction of the 1- and 2-axis, respectively, and its conductivity is σ_4 . If numbers of the combined unit shown in Fig. 8b are placed side by side, then the model shown in Fig. 8a can be constructed. Similar to case 2, the macroscopic equivalent conductivities along three principal directions can be derived as:

$$\sigma_{11} = \frac{(d_{x1} + d_{x2})}{(d_{y1} + d_{y2})} \left[\frac{\sigma_4\sigma_1d_{y1}}{\sigma_4d_{x1} + \sigma_1d_{x2}} + \frac{\sigma_2\sigma_3d_{y2}}{\sigma_3d_{x1} + \sigma_2d_{x2}} \right], \tag{45a}$$

$$\sigma_{22} = \frac{(d_{y1} + d_{y2})}{(d_{x1} + d_{x2})} \left[\frac{\sigma_1\sigma_2d_{x1}}{\sigma_2d_{y1} + \sigma_1d_{y2}} + \frac{\sigma_3\sigma_4d_{x2}}{\sigma_3d_{y1} + \sigma_4d_{y2}} \right], \tag{45b}$$

$$\sigma_{33} = \frac{d_{y1}(\sigma_1d_{x1} + \sigma_4d_{x2}) + d_{y2}(\sigma_3d_{x2} + \sigma_2d_{x1})}{(d_{x1} + d_{x2})(d_{y1} + d_{y2})}. \tag{45c}$$

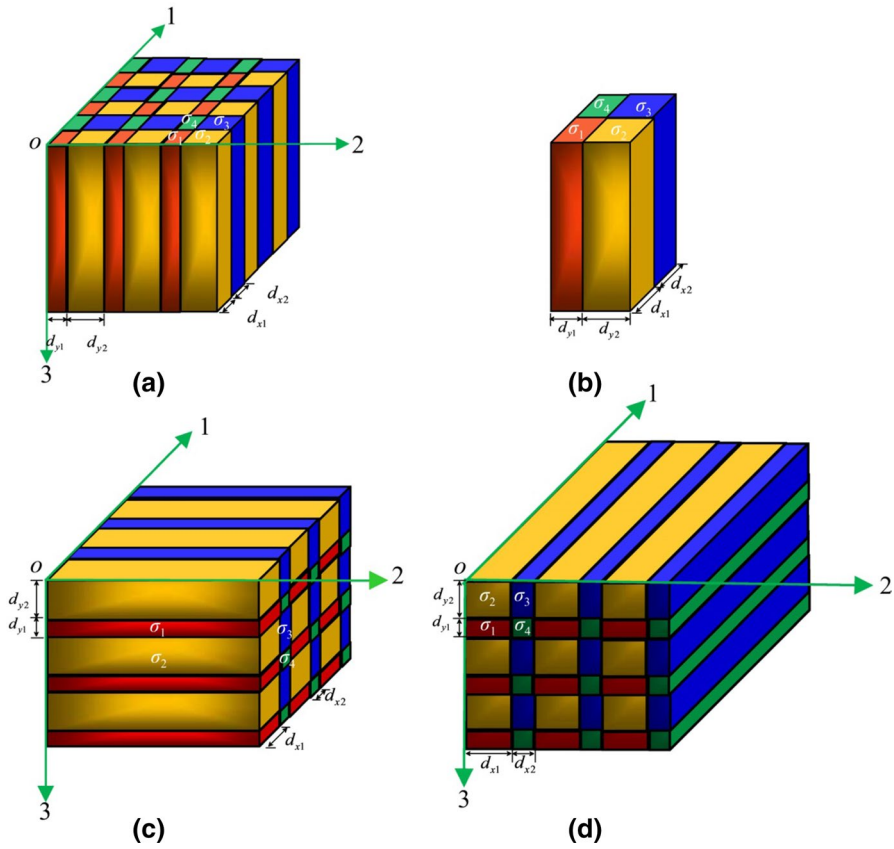


Fig. 8 Geometric graph representation of the more general biaxial anisotropic conductivity tensor (case 3) given by Eqs. (43a–c) and (45a–c) in the principal axis coordinate system. The model **a** can be considered as infinitely repeated VTI, and models **c** and **d** are infinitely repeated HTI. The graph in panel **a** is composed of many sets of rectangular prisms with different conductivities. Each set of prisms consists of four cubes in different colors shown in subfigure **(b)**. The geometric graphs shown in subfigure **c** and **d** can be obtained from the geometric graph **a** being rotated 90° around the *x*- and *y*-axis, respectively

The models shown in Fig. 8c, d can be considered as the ones obtained when the model in Fig. 8a is rotated 90° around the 1- and 2-axis, respectively. Therefore, the macroscopic equivalent conductivity for these models can be calculated by substituting Eqs. (45a–c) into Eqs. (43a–c).

It should be noted that the result in this case will reduce to the previous result in case 2 when $\sigma_1 = \sigma_3$.

6.4 Case 4: Biaxial Anisotropy with Periodically Varied HTI/VTI

Now we consider a more general biaxial anisotropy which is constructed by periodically varied HTI/VTI rectangular prisms. In this situation, the conductivity varies in the 1, 2, 3 directions, as shown in Fig. 9a. In order to construct this model, two sets of the combination of four blocks with different dimensions and conductivities shown in Fig. 9b and c,

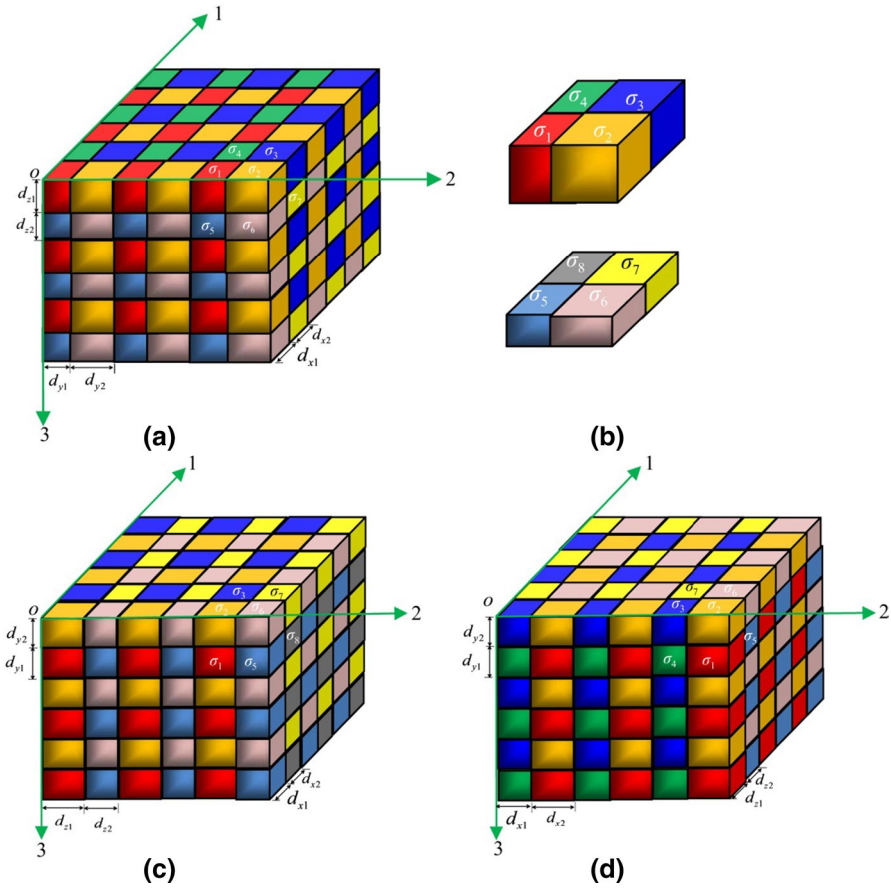


Fig. 9 Geometric graph representation of the generally biaxial anisotropic conductivity tensor (case 4) given by Eqs. (43a–c) and (46a–c) in the principal axis coordinate system. The graph in panel **a** consists of many sets of rectangular prisms with different conductivities, arranged alternately side by side. Each set of prisms is composed of eight cubes in different colors shown in subfigure **(b)**. The geometric graphs shown in subfigure **c** and **d** can be considered as the ones obtained when the geometric graph **a** is rotated 90° around the *x*- and *y*-axis, respectively

respectively, are superposed to form a basic unit model, which are then placed side by side to construct the final anisotropic model.

In Fig. 9b, the red rectangular prism has the dimension of d_{x1} and d_{y1} in the direction of the 1- and 2-axis, respectively, and its conductivity is σ_1 . The yellow rectangular prism has the dimension of d_{x1} and d_{y2} in the direction of the 1- and 2-axis, respectively, and its conductivity is σ_2 . The blue rectangular prism has the dimension of d_{x2} and d_{y2} in the direction of the 1- and 2-axis, respectively, and its conductivity is σ_3 . The green rectangular prism has the dimension of d_{x2} and d_{y1} in the direction of the 1- and 2-axis, respectively, and its conductivity is σ_4 . The thicknesses of these four rectangular prisms are d_{z1} .

In Fig. 9c, the thicknesses of all the blocks are d_{z2} . The light blue rectangular prism has the dimension of d_{x1} and d_{y1} in the direction of the 1- and 2-axis, respectively, and its conductivity is σ_5 . The dark pink rectangular prism has the dimension of d_{x1} and d_{y2} in the direction of the 1- and 2-axis, respectively, and its conductivity is σ_6 . The light yellow

rectangular prism has the dimension of d_{x2} and d_{y2} in the direction of the 1- and 2-axis, respectively, and its conductivity is σ_7 . The light gray rectangular prism has the dimension of d_{x2} and d_{y1} in the direction of the 1- and 2-axis, respectively, and its conductivity is σ_8 .

Therefore, the conductivity of the basic unit model composed of the eight blocks can be regarded as the macroscopic conductivity of the model. Using a calculation method similar to the previous cases, the equivalent macroscopic conductivity of this model can be calculated by

$$\sigma_{11} = \frac{(d_{x1} + d_{x2})}{(d_{y1} + d_{y2})(d_{z1} + d_{z2})} \left[\frac{\sigma_1 \sigma_4 d_{y1} d_{z1}}{\sigma_4 d_{x1} + \sigma_1 d_{x2}} + \frac{\sigma_2 \sigma_3 d_{y2} d_{z1}}{\sigma_3 d_{x1} + \sigma_2 d_{x2}} + \frac{\sigma_5 \sigma_8 d_{y1} d_{z2}}{\sigma_8 d_{x1} + \sigma_5 d_{x2}} + \frac{\sigma_6 \sigma_7 d_{y1} d_{z2}}{\sigma_7 d_{x1} + \sigma_6 d_{x2}} \right], \quad (46a)$$

$$\sigma_{22} = \frac{(d_{y1} + d_{y2})}{(d_{x1} + d_{x2})(d_{z1} + d_{z2})} \left[\frac{\sigma_1 \sigma_2 d_{x1} d_{z1}}{\sigma_2 d_{y1} + \sigma_1 d_{y2}} + \frac{\sigma_3 \sigma_4 d_{x2} d_{z1}}{\sigma_3 d_{y1} + \sigma_4 d_{y2}} + \frac{\sigma_5 \sigma_6 d_{x1} d_{z2}}{\sigma_6 d_{y1} + \sigma_5 d_{y2}} + \frac{\sigma_7 \sigma_8 d_{x2} d_{z2}}{\sigma_7 d_{y1} + \sigma_8 d_{y2}} \right], \quad (46b)$$

$$\sigma_{33} = \frac{(d_{z1} + d_{z2})}{(d_{x1} + d_{x2})(d_{y1} + d_{y2})} \left[\frac{\sigma_1 \sigma_5 d_{x1} d_{y1}}{\sigma_5 d_{z1} + \sigma_1 d_{z2}} + \frac{\sigma_2 \sigma_6 d_{x1} d_{y2}}{\sigma_6 d_{z1} + \sigma_2 d_{z2}} + \frac{\sigma_3 \sigma_7 d_{x2} d_{y2}}{\sigma_7 d_{z1} + \sigma_3 d_{z2}} + \frac{\sigma_4 \sigma_8 d_{x2} d_{y1}}{\sigma_8 d_{y1} + \sigma_4 d_{y2}} \right]. \quad (46c)$$

As in cases 2, 3 and 4, a number of studies (Madden 1976; Schmeling 1986; Bahr 1997; Bigalke 1999, 2000b; Kozlovskaya and Hjelt 2000; Pervukhina et al. 2005; Wannamaker 2005; Semeriyarov et al. 2009; Pommier 2014; Kirkby and Heinson 2017) have considered the macroscopic anisotropy of the Earth's medium with the form of 2-D or 3-D random networks and to give the corresponding formulas. However, their geometric forms and formulas are relatively complicated and thus inconvenient to extensively be applied to test modeling and inversion programs. Therefore, we have presented some simpler theoretical models and formulas in order to conveniently calculate the macroscopic anisotropic conductivity tensor. Although no practical application examples are given in this work, it is foreseeable that these concise formulas can be used in conductivity. These expressions would play an important role in greatly reducing the inverted parameters in the inversion of the anisotropic conductivities.

One may find that the case 4 should reduce to the case 3 if $\sigma_1 = \sigma_5$, $\sigma_2 = \sigma_6$, $\sigma_3 = \sigma_7$ and $\sigma_4 = \sigma_8$.

7 Synthetic Examples

In previous three sections, we have presented three types of graphical representations of the conductivity tensor (i.e., ellipsoid, Mohr circle and geometric form). The use of the representation in terms of sheet and prism models is a little bit philosophically different from the representation in terms of ellipsoids and Mohr circles.

Typically, the geometrical models will be used to represent a physical situation or to provide an example of an anisotropic medium, whereas the ellipsoidal and Mohr circles are simple graphical representations of the anisotropic conductivity tensor. The ellipsoidal and Mohr circle representations provide a unique representation of an arbitrary anisotropic conductivity, and it can be easily constructed for a specified conductivity tensor. In contrast, the geometric models do not provide a unique representation and it may be more difficult (or impossible) to construct a model corresponding to an arbitrary tensor.

In this section, we will provide synthetic examples to illustrate them so as to help one to understand these graphical representations of the conductivity tensor. Since the arbitrary conductivity tensor in measurement coordinate system can be diagonalized through appropriately rotating the coordinate system (c.f., section 4), our synthetic examples will concentrate mainly on the diagonal conductivity tensor in the principal axis coordinate system. However, results in an arbitrary coordinate can be obtained using an appropriate rotation matrix. For a given conductivity tensor in arbitrary coordinate (or measuring coordinate) system, the tensor can be diagonalized by using Eq. (11) or by Eqs. (20)–(22). The graphical representations of the tensor with Mohr circle and ellipsoid are completely equivalent to the case of the diagonal conductivity tensor. However, the third representation (i.e., geometric form representation) does not exist for a given arbitrary tensor, since its geometric model parameters cannot be uniquely determined in advance, and there may be an infinite number of possible geometrical forms. Four synthetic examples will be shown based on the cases described in Sect. 6, with some possible numerical values assigned in order to make the graphical representations of the conductivity tensor better understood. The values of the conductivity tensor will be firstly derived according to the closed-form expressions, and then, the conductivity tensor will be graphically represented with both the ellipsoid and Mohr circles in different coordinate systems.

7.1 Case 1

In this case, we will examine the macroscopic anisotropic conductivity of the model shown in Fig. 10c consisting of two thin layers with different thicknesses and resistivities, which is just the basic set construct the model shown in Fig. 6a. For the sake of convenience, the units will be omitted in the following formulas and figures. Hence, according to Eqs. (41) and (42), the anisotropic conductivity tensor given in (40a) is

$$\sigma = \begin{bmatrix} \sigma_{xx} & 0 & 0 \\ 0 & \sigma_{yy} & 0 \\ 0 & 0 & \sigma_{zz} \end{bmatrix} = \begin{bmatrix} 0.07 & 0 & 0 \\ 0 & 0.07 & 0 \\ 0 & 0 & 0.025 \end{bmatrix}. \tag{47}$$

Therefore, the figure shown in Fig. 10c is an equivalent geometric form representation of the anisotropic conductivity tensor given in Eq. (47). As stated in the previous sections, this anisotropic conductivity tensor can also be represented with Mohr circle and 3-D ellipsoid; the corresponding representations are shown in Fig. 10a, b, respectively.

It can be seen from Fig. 10a that the value of σ_{13} equal to that of σ_{23} [according to Eqs. (30) and (31)] and the centers O_1 and O_3 coincide with each other (according to Eqs. (33) and (35)); hence, the first two circles (which should be shown in blue and green, respectively) coincide with each other and only the blue circle appears. It is also clear that σ_{12} equals to zero according to Eq. (32), and thus, the third circle (which should be shown in cyan) reduces to a point (i.e., the center O_2).

The discussion above is conducted in the principal axis coordinate system; now we examine the situation in an arbitrary coordinate system (say, $o\text{-}xyz$ coordinate system) to check what will happen when the tensor is rotated. For a given rotation matrix

$$\mathbf{R} = \begin{bmatrix} 0.5000 & -0.8660 & 0 \\ 0.6124 & 0.3536 & -0.7071 \\ 0.6124 & 0.3536 & 0.7071 \end{bmatrix} = \begin{bmatrix} \cos(60^\circ) & \cos(150^\circ) & \cos(90^\circ) \\ \cos(52.2^\circ) & \cos(69.3^\circ) & \cos(135^\circ) \\ \cos(52.2^\circ) & \cos(69.3^\circ) & \cos(45^\circ) \end{bmatrix},$$

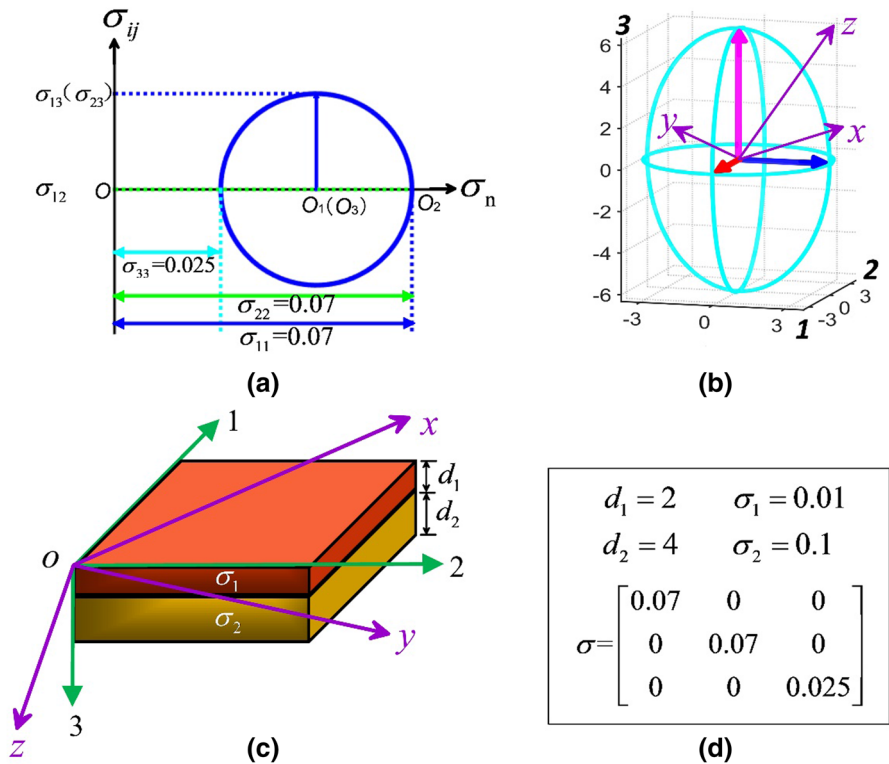


Fig. 10 Graphical representation with the Mohr circle (a), the 3-D ellipsoid (b) and the geometric graph (c) of the conductivity tensor given in panel (d). The conductivities of these two different thin layers shown in c are assigned as 0.01 and 0.1 S/m (i.e., $\sigma_1 = 0.01\text{S/m}$, $\sigma_2 = 0.1\text{S/m}$), respectively, and their thickness is 2 and 4 m (i.e., $d_1 = 2\text{m}$ and $d_2 = 4\text{m}$), respectively. These parameters are listed at the top of the panel (d). The calculated microscopic anisotropic conductivity tensor based on the Ohm’s law from the geometric model c is given at the bottom of the panel (d). The arbitrary coordinate system (say, o - xyz coordinate system) is shown by the purple arrows in panels (b) and (c), while the anisotropic principal coordinate system is marked by o -123. It should be noted the different dimension scale between the 1- and 2-axis in panel (b)

the intersection angles between the 1- and x -axis, 2- and y -axis, 3- and z -axis are 60° , 69.3° and 45° , respectively. The arbitrary coordinate system (say, o - xyz coordinate system) is shown by the purple arrows in Figs. 10b, c. Then, one may obtain the conductivity tensor $\bar{\sigma}$ in a given arbitrary coordinate system using Eq. (11); the resulting tensor is as follows:

$$\bar{\sigma} = \begin{bmatrix} 0.07 & 0 & 0 \\ 0 & 0.0475 & 0.0225 \\ 0 & 0.0225 & 0.0475 \end{bmatrix}.$$

For the given conductivity tensor, the differences between the principal axes (o -1, 2, 3) and arbitrary coordinate systems (o - xyz) are self-explanatory in Fig. 10b, c when the tensor is graphically represented with the 3-D ellipsoid and the geometric form.

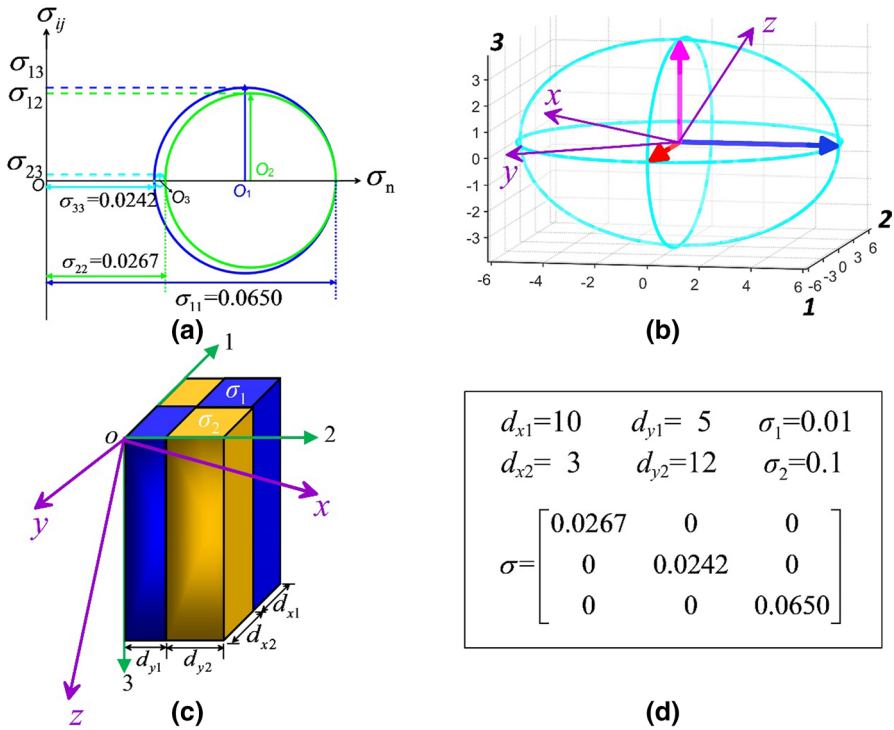


Fig. 11 Graphical representation with the Mohr circle (a), the 3-D ellipsoid (b) and the geometric model (c) of the conductivity tensor given in panel (d). The conductivity tensor is calculated according to the Ohm’s law from the geometric graph (c) with the conductivities and thicknesses of the values listed at the top of the panel (d). See the text in section for details. The conductivity values of two different media shown in blue and yellow prisms are assigned as 0.01 and 0.1 S/m (i.e., $\sigma_1 = 0.01\text{S/m}$, $\sigma_2 = 0.1\text{S/m}$), respectively. Their thicknesses are 10 and 3 m (i.e., $d_{x1} = 10\text{m}$ and $d_{x2} = 3\text{m}$) while their widths are 5 and 12 m (i.e., $d_{y1} = 5\text{m}$ and $d_{y2} = 12\text{m}$). The arbitrary coordinate system (say, $o\text{-}xyz$ coordinate system) is shown by the purple arrows in panels (b) and (c), while the anisotropic principal coordinate system is marked by $o\text{-}123$. It should be noted the different dimension scale between the 1- and 2-axis in panel (b)

7.2 Case 2

Here, the macroscopic anisotropic conductivity of the model described in Fig. 11c will be treated. This model is composed of four rectangular prisms involving two different media of different resistivities. The four prisms may have different dimensions and infinitely extend along the 1-, 2-, 3-axis. This model can be regarded as a basic set of infinitely rectangular prisms to be repeatedly arranged to construct the model shown in Fig. 7a.

Then, based on Eqs. (44a–c), the anisotropic conductivity tensor listed in Eq. (43a) can be derived as

$$\sigma = \begin{bmatrix} \sigma_{11} & 0 & 0 \\ 0 & \sigma_{22} & 0 \\ 0 & 0 & \sigma_{33} \end{bmatrix} = \begin{bmatrix} 0.0267 & 0 & 0 \\ 0 & 0.0242 & 0 \\ 0 & 0 & 0.0650 \end{bmatrix}. \tag{48}$$

This anisotropic conductivity tensor is also listed in the panel (d) in Fig. 11. Correspondingly, the three graphical representations with the Mohr circle, the 3-D ellipsoid and the geometric form of the anisotropic conductivity tensor given in Eq. (48) are shown in Fig. 11a–c, respectively.

We have discussed the case in the principal axis coordinate system; now the situation in an arbitrary coordinate system (say, σ -xyz coordinate system) will be conducted to examine what will happen when the tensor is rotated. For a given rotation matrix

$$\mathbf{R} = \begin{bmatrix} -0.7866 & -0.0795 & 0.6124 \\ 0.3624 & -0.8624 & 0.3536 \\ 0.5000 & 0.5000 & 0.7071 \end{bmatrix} = \begin{bmatrix} \cos(141.9^\circ) & \cos(94.6^\circ) & \cos(52.2^\circ) \\ \cos(68.8^\circ) & \cos(149.6^\circ) & \cos(69.3^\circ) \\ \cos(60^\circ) & \cos(60^\circ) & \cos(45^\circ) \end{bmatrix},$$

the intersection angles between the 1- and x -axis, 2- and y -axis, 3- and z -axis are 141.9° , 149.6° and 45° , respectively. The arbitrary coordinate system (say, σ -xyz coordinate system) is indicated by the purple arrows in Figs. 11b and 11c. Then, using Eq. (11), the conductivity tensor $\bar{\sigma}$ in a given arbitrary coordinate system may be calculated as follows:

$$\bar{\sigma} = \begin{bmatrix} 0.0410 & 0.0081 & 0.0167 \\ 0.0081 & 0.0296 & 0.0107 \\ 0.0167 & 0.0107 & 0.0452 \end{bmatrix}.$$

For the given conductivity tensor, when it is graphically represented with the 3-D ellipsoid and the geometric form, one may easily find the differences between the principal axes (σ -1, 2, 3) and arbitrary coordinate systems (σ -xyz) in Fig. 11b and 11c.

7.3 Case 3

In this section, we investigate the macroscopic anisotropic conductivity of the model described in Fig. 12b consisting of four rectangular prisms with different dimensions and conductivities extending infinitely along the 1-, 2-, 3-axis. This model is just the basic set of the prisms to be used to construct the model shown in Fig. 8a.

And then for the model shown in Fig. 12b, the macroscopic conductivity in Eq. (43a) can be easily obtained from Eqs. (45aa–c); the result is listed as

$$\bar{\sigma} = \begin{bmatrix} \sigma_{11} & 0 & 0 \\ 0 & \sigma_{22} & 0 \\ 0 & 0 & \sigma_{33} \end{bmatrix} = \begin{bmatrix} 0.00018 & 0 & 0 \\ 0 & 0.0055 & 0 \\ 0 & 0 & 0.0116 \end{bmatrix}. \tag{49}$$

This anisotropic conductivity tensor is also shown in the panel (c) in Fig. 12. Accordingly, the three graphical representations with the Mohr circle, the 3-D ellipsoid and the geometric form of the anisotropic conductivity tensor given in Eq. (49) are shown in Fig. 12a, b, d, respectively.

After investigating the situation in the principal axis coordinate system, we further treat the case in an arbitrary coordinate system (say, σ -xyz coordinate system) to examine the variation in the rotated tensor. For a given rotation matrix

$$\mathbf{R} = \begin{bmatrix} 0.7866 & -0.3624 & 0.5000 \\ 0.0795 & 0.8624 & 0.5000 \\ -0.6124 & -0.3536 & 0.7071 \end{bmatrix} = \begin{bmatrix} \cos(38.1^\circ) & \cos(111.2^\circ) & \cos(60^\circ) \\ \cos(85.4^\circ) & \cos(30.4^\circ) & \cos(60^\circ) \\ \cos(127.8^\circ) & \cos(110.7^\circ) & \cos(45^\circ) \end{bmatrix},$$

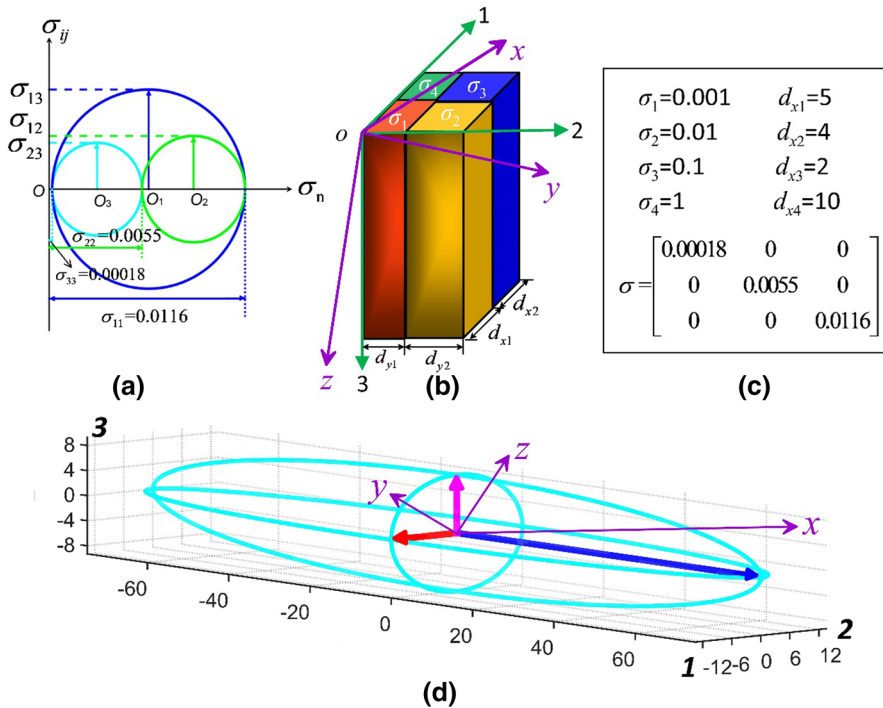


Fig. 12 Graphical representation with the Mohr circle (a), the geometric graph (b) and the 3-D ellipsoid (d) of the conductivity tensor given in panel (c). The conductivity tensor is calculated according to the Ohm’s law from the geometric model (b) with the conductivities and thicknesses of the values listed at the top of the panel (c). The corresponding conductivities and sizes of the four adjacent prisms in panel (b) are given in panel (d) and also listed as follows: $\sigma_1 = 0.001\text{S/m}$, $\sigma_2 = 0.01\text{S/m}$, $\sigma_3 = 0.1\text{S/m}$, $\sigma_4 = 1\text{S/m}$; $d_{x1} = 5\text{m}$, $d_{x2} = 4\text{m}$, $d_{y1} = 2\text{m}$, $d_{y2} = 10\text{m}$. The arbitrary coordinate system (say, $o\text{-}xyz$ coordinate system) is shown by the purple arrows in panels (b) and (d), while the anisotropic principal coordinate system is marked by $o\text{-}123$. It should be noted the different dimension scale between the 1- and 2-axis in panel (b)

the angles between the 1- and x -axis, 2- and y -axis, 3- and z -axis are 38.1° , 30.4° and 45° , respectively. The arbitrary coordinate system (say, $o\text{-}xyz$ coordinate system) is represented by the purple arrows in Fig. 12b, d. Then, through Eq. (11), one can obtain the conductivity tensor $\bar{\sigma}$ in a given arbitrary coordinate system. The conductivity tensor can be written as follows:

$$\bar{\sigma} = \begin{bmatrix} 0.0037 & 0.0012 & 0.0047 \\ 0.0012 & 0.0070 & 0.0024 \\ 0.0047 & 0.0024 & 0.0066 \end{bmatrix}$$

For the above conductivity tensor, the differences between the 3-D ellipsoid (the geometric form) representations in the principal axes ($o\text{-}1, 2, 3$) and that in an arbitrary coordinate system ($o\text{-}xyz$) in Fig. 12b (Fig. 12d) are very obvious.

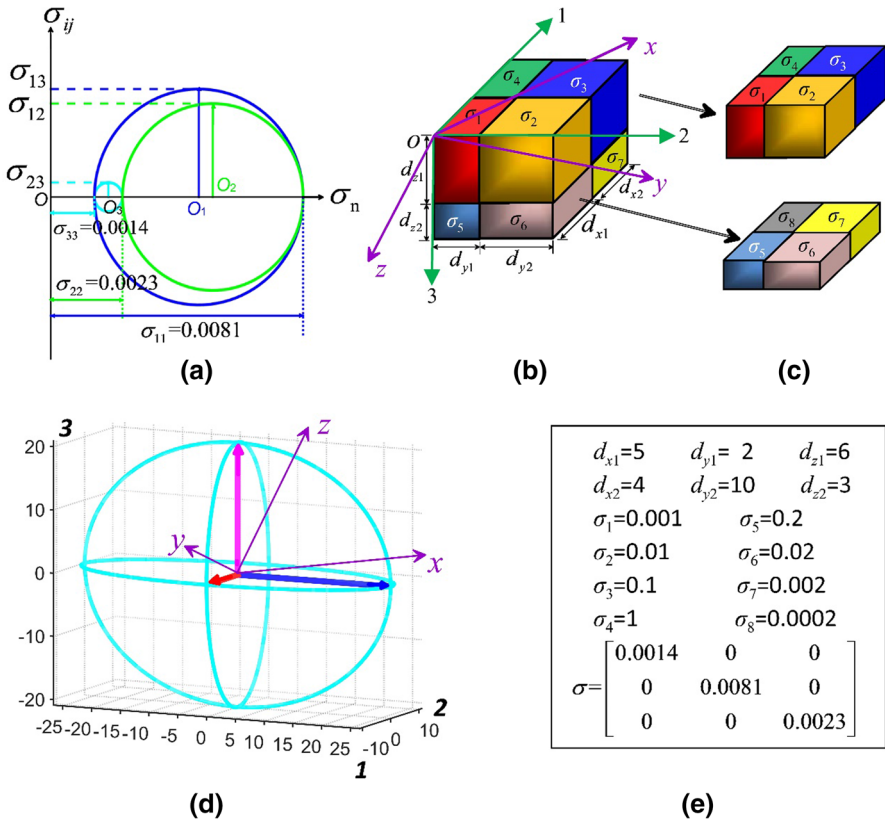


Fig. 13 Graphical representation with the Mohr circle (a), the geometric graph (b) and the 3-D ellipsoid (d) of the conductivity tensor given in panel (e). The geometric model (b) consists of eight cubes shown in panel (c). The conductivity tensor is calculated according to the Ohm’s law from the geometric graph (b) with the conductivities and thicknesses of the values listed at the top of the panel (e). The conductivities and sizes of the eight cubes are listed as follows: $\sigma_1 = 0.0001\text{S/m}$, $\sigma_2 = 0.001\text{S/m}$, $\sigma_3 = 0.01\text{S/m}$, $\sigma_4 = 0.1\text{S/m}$; $\sigma_5 = 0.2\text{S/m}$, $\sigma_6 = 0.02\text{S/m}$, $\sigma_7 = 0.002\text{S/m}$, $\sigma_8 = 0.0002\text{S/m}$; $d_{x1} = 5\text{m}$, $d_{x2} = 4\text{m}$, $d_{y1} = 2\text{m}$, $d_{y2} = 10\text{m}$, $d_{z1} = 6\text{m}$, $d_{z2} = 3\text{m}$. The arbitrary coordinate system (say, $o\text{-}xyz$ coordinate system) is shown by the purple arrows in panels (b) and (d), while the anisotropic principal coordinate system is marked by $o\text{-}123$. It should be noted the different dimension scale between the 1- and 2-axis in panel (d)

7.4 Case 4

In this case, we will consider the macroscopic anisotropic conductivity of the model described in Fig. 13b, which is composed of eight cubes in different colors as shown in the panel (c). This model is just the basic set of cubes to construct the model shown in Fig. 9a. The conductivities and sizes of the eight cubes may have different values with each other.

Then, we can easily calculate the macroscopic conductivity of the model shown in Fig. 13b from Eqs. 43(a) and (46a–c); the resulting conductivity tensor is

$$\sigma = \begin{bmatrix} \sigma_{11} & 0 & 0 \\ 0 & \sigma_{22} & 0 \\ 0 & 0 & \sigma_{33} \end{bmatrix} = \begin{bmatrix} 0.0014 & 0 & 0 \\ 0 & 0.0081 & 0 \\ 0 & 0 & 0.0023 \end{bmatrix} \tag{50}$$

This conductivity tensor in Eq. (50) (also shown in the panel (e) in Fig. 13) is then graphically represented with Mohr circle, the 3-D ellipsoid and the geometric form, which are shown in Figs. 13a, b, d, respectively.

The situation in the principal axis coordinate system (σ -1, 2, 3) has been investigated; now we further examine the case of the rotated conductivity tensor in an arbitrary coordinate system (say, σ -xyz coordinate system) to see what will happen. For a given rotation matrix

$$\mathbf{R} = \begin{bmatrix} 0.8536 & 0.1464 & 0.5000 \\ 0.1464 & 0.8536 & -0.5000 \\ -0.5000 & 0.5000 & 0.7071 \end{bmatrix} = \begin{bmatrix} \cos(31.4^\circ) & \cos(81.6^\circ) & \cos(60^\circ) \\ \cos(81.6^\circ) & \cos(31.4^\circ) & \cos(120^\circ) \\ \cos(120^\circ) & \cos(60^\circ) & \cos(45^\circ) \end{bmatrix},$$

the intersection angles between the 1- and x -axis, 2- and y -axis, 3- and z -axis are 31.4° , 31.4° and 45° , respectively. The arbitrary coordinate system (say, σ -xyz coordinate system) is shown by the purple arrows in Fig. 13b, d. Then, the conductivity tensor $\bar{\sigma}$ in a given arbitrary coordinate system may be calculated by Eq. (11) as follows:

$$\bar{\sigma} = \begin{bmatrix} 0.0018 & 0.0006 & 0.0008 \\ 0.0006 & 0.0065 & 0.0025 \\ 0.0008 & 0.0025 & 0.0035 \end{bmatrix}.$$

For this conductivity tensor, the difference between the graphical representation with the geometric form (or the 3-D ellipsoid) in the principal axes (σ -1, 2, 3) and that in an arbitrary coordinate system (σ -xyz) in Fig. 13b (or Fig. 13d) are very clear.

8 Discussion

From the previous descriptions and synthetic examples about graphical representations of symmetric conductivity tensor in anisotropic media, we can get the following remarks:

1. In 2-D case, Mohr circle provides a graphic representation of a tensor as a function of the rotation of the coordinate system. The elements of the conductivity tensor can be directly determined by the position of the circle. In 3-D case, Mohr circle representation of the conductivity tensor is conducted through three 2-D Mohr circles in the same plane. As mentioned in Sect. 5, the drawing of the Mohr circle is performed in the principal coordinate system. Therefore, for an arbitrary symmetric conductivity tensor, it is diagonalized as the measurement coordinate system is rotated to the principal coordinate system, the drawing of its 3-D Mohr circle representation is the same as that of the diagonal tensor, but it is very difficult to show the elements of the arbitrary tensor in the Mohr circle, except that one of the measuring axes is the same as one of the principal axes. However, these elements can be easily calculated from Eqs. (9) and (11) based on the 3-D Mohr circle. For the ellipsoid representation of a given conductivity tensor, it can be uniquely determined by all elements of a given conductivity tensor and can visually represent the spatial variation in conductivity anisotropy in the principal axis coordinate system. However, the coordinates of a point on the ellipsoidal surface do not directly represent all the elements of the conductivity tensor. The elements of the conductivity tensor in any coordinate system can be determined by the coordinates of this point based on the other conditions. Therefore, the determination of the conductivity tensor elements

in any coordinate system by the ellipsoid representation is not as convenient as by the Mohr circle. This may be the main reason why the Mohr circle representations obtain a wider application than the ellipsoid representation in stress tensor analysis. In the stress tensor analysis, the Mohr circle indicates that the maximum and minimum stresses and shear stress can be calculated very conveniently. Also in the Mohr circle representation of the conductivity tensor, the maximum and minimum resistivities and the other tensor elements in any coordinate system can be obtained simply and conveniently. In this respect, the Mohr circle representation is superior to the ellipsoid representation.

2. When two elements of the conductivity tensor are equal, their corresponding Mohr circles coincide with each other (for example, Fig. 10a indicates the Mohr circle of the HTI medium). The ellipsoidal surface represents the conductivity anisotropy in a 3-D space, which can more intuitively indicate the principal directions of the anisotropy (for example, Fig. 10b clearly indicates the anisotropy in the vertical direction). When indicating the anisotropy principal directions, the ellipsoid representation is more intuitive and direct than the Mohr circle (as the case shown in Fig. 11a, b, for example). Therefore, Mohr circle representation of the conductivity tensor is superior to the ellipsoid for showing the relative size of the three principle conductivities more clearly for the case when two of the values are very similar and therefore for distinguishing uniaxial and biaxial anisotropy.
3. The Mohr circle representation of the stress tensor has been widely used in practice. Although the Mohr circle of the conductivity tensor has not been paid much attention by now, it is possible to establish some related links between the Mohr circle of the stress tensor and that of the conductivity tensor to promote researches on electrical anisotropy. In this point, it seems that the ellipsoid representation is not as convenient as the Mohr circle representation.
4. The geometrical form representation of the conductivity tensor (Figs. 10c, 11c, 12b and 13b) directly represents the microscopic anisotropic structure using an equivalent homogeneous isotropic rectangular prism combination, which links the macroscopic anisotropy with the microscopic anisotropy. At the same time, the macroscopic anisotropy structures can be equivalently expressed by various combinations of isotropic rectangular prism, which makes the anisotropic conductivity tensor be analytically expressed by simple formula. This in turn allows the anisotropic conductivity structure to be replaced by an isotropic model, so that the isotropic numerical simulation program can be used to simulate the responses of the anisotropic model, and thus, it provides another way to quantitatively simulate (with regard the simulation of the anisotropic response with an isotropic model, we will discuss separately in another paper). However, for a given conductivity tensor, the Mohr circle representation and the ellipsoid representation are unique, while the geometric form representation is not unique. And the conductivity tensor and its geometric form representations are not one-to-one correspondence. This representation can only be conducted for a specific anisotropic structure, and its drawing is more complicated and cumbersome than the other two graphical representations. In addition, the four geometric form representations listed in this work are just some of the simplest geometric form representations of given conductivity tensors. Obviously there may be many other more complicated geometric form representations.

9 Conclusions

Three graphical representations (i.e., ellipsoid and Mohr circle as well as equivalent geometric form) for symmetric conductivity tensor of the anisotropic medium in the principal axis coordinate system are presented.

In the principal axis coordinate system, three principal components of the conductivity tensor can be represented by lengths of three semi-axes of the ellipsoid. The flatness or ellipticity of the ellipsoid reflects the anisotropic behaviors of the conductivity tensor. The higher the ellipticity of the conductivity tensor ellipsoid, the more obvious the electrical anisotropy features. When the ellipsoid degenerates into a circle, the conductivity of the medium becomes completely isotropic. The conductivity tensor can also be represented by the Mohr circle. The radius of the Mohr circle reflects the differences in conductivities along the anisotropic principal axes. The Mohr circle can also graphically indicate the variation in the elements of the conductivity tensor with the coordinate system. For the third graphical representation, i.e., an equivalent geometric form representation of the conductivity tensor, several conductivity tensor models of anisotropic media are illustrated and explained. In addition, the formulas used to calculate the macroscopic conductivity for those media are also given. The present work provides convenient tools to quantitatively study the features of the electrical anisotropy in Earth.

Acknowledgements The research was supported by the National Natural Science Foundation of China (Grant Nos. 41474054, 40774035 and 41776079). The authors thank Dr. Pilar Queralt (Editor) and two reviewers Dr. Ian Ferguson and Dr. Anna Martí for their thorough reading of the manuscript and for their insightful comments and constructive suggestions which certainly improved the quality of this paper.

References

- Adetunji AQ, Ferguson II, Jones AG (2015) Reexamination of magnetotelluric responses and electrical anisotropy of the lithospheric mantle in the Grenville Province, Canada. *J Geophys Res Solid Earth* 120(3):1890–1908
- Atkinson G (1967) An approximate flow equation for geomagnetic flux tubes and its application to polar substorms. *J Geophys Res* 72(21):5373–5382
- Baba K, Chave AD, Evans RL, Hirth G, Mackie RL (2006) Mantle dynamics beneath the East Pacific Rise at 17 degrees S: Insights from the mantle electromagnetic and tomography (MELT) experiment. *J Geophys Res-Solid Earth*. <https://doi.org/10.1029/2004jb003598>
- Bahr K (1997) Electrical anisotropy and conductivity distribution functions of fractal random networks and of the crust: the scale effect of connectivity. *Geophys J Int* 130(3):649–660. <https://doi.org/10.1111/j.1365-246X.1997.tb01859.x>
- Bahr K, Duba A (2000) Is the asthenosphere electrically anisotropic? *Earth Planet Sci Lett* 178(1):87–95. [https://doi.org/10.1016/S0012-821X\(00\)00070-4](https://doi.org/10.1016/S0012-821X(00)00070-4)
- Bahr K, Smirnov M, Steveling E (2002) A gelation analogy of crustal formation derived from fractal conductive structures. *J Geophys Res: Solid Earth* 107(B11):ECV-18
- Baker WG, Martyn D (1953) The electric current in the ionosphere, part 1, the conductivity. *Phil.trans.r.soc. lond.a*, 246
- Bigalke J (1999) Investigation of the conductivity of random networks. *Phys A* 272(3–4):281–293
- Bigalke J (2000a) Derivation of an equation to calculate the average conductivity of random networks. *Phys A* 285(3–4):295–305
- Bigalke J (2000b) A study concerning the conductivity of porous rock. *Phys Chem Earth Part A* 25(2):189–194
- Börner JH, Girault F, Bhattarai M, Adhikari LB, Deldicque D, Perrier F et al (2018) Anomalous complex electrical conductivity of a graphitic black schist from the Himalayas of central Nepal. *Geophys Res Lett* 45(9):3984–3993

- Chapagain NP (2016) Ionospheric plasma drift and neutral winds modeling. *Res J Phys Sci* 4(7):5–10
- Cowling TG (1945) The electrical conductivity of an ionized gas in a magnetic field, with applications to the solar atmosphere and the ionosphere. *Proc R Soc A Math Phys Eng Sci* 183(183):453–479
- Culmann C (1866) *Die graphische statik* (vol 1). Meyer & Zeller
- Davydycheva S, Wang T (2011) Modeling of electromagnetic logs in a layered, biaxially anisotropic medium. In SEG technical program expanded abstracts 2011. Society of Exploration Geophysicists, pp 494–498
- Dekker DL, Hastie LM (1980) Magneto-telluric impedances of an anisotropic layered Earth model. *Geophys J R Astron Soc* 61(1):11–20
- Du Frane WL, Roberts JJ, Toffelmier DA, Tyburczy JA (2005) Anisotropy of electrical conductivity in dry olivine. *Geophys Res Lett* 32(24)
- Eisel M, Haak V (1999) Macro-anisotropy of the electrical conductivity of the crust: a magnetotelluric study of the German Continental Deep Drilling site (KTB). *Geophys J Int* 136(1):109–122. <https://doi.org/10.1046/j.1365-246X.1999.00707.x>
- Everett ME, Constable S (1999) Electric dipole fields over an anisotropic seafloor: theory and application to the structure of 40 Ma Pacific Ocean lithosphere. *Geophys J Int* 136(1):41–56. <https://doi.org/10.1046/j.1365-246X.1999.00725.x>
- Falae PO, Kanungo D, Chauhan P, Dash RK (2019) Recent trends in Application of electrical resistivity tomography for landslide study. In: Renewable energy and its innovative technologies. Springer, Berlin, pp 195–204
- Ferdinand PB, Johnson ER (1992) *Mechanics of materials*. McGraw-Hill, New York
- Feynman RP, Leighton RB, Sands M, Hafner EM (1965) *The Feynman lectures on physics*, vol II. Addison-Wesley Publishing, Reading
- Gololobov DV, Malevich IY (2005). Physical and electrochemical processes in the medium above the hydrocarbon deposit, Reports of the Belarusian State University of Informatics and Radioelectronics, (1 (9), (In Russian). (Vol. 1(9))
- Grant FS, West GF (1965) *Interpretation theory in applied geophysics*. McGraw-Hill, New York
- Greenhalgh S, Zhou B, Greenhalgh M, Marescot L, Wiese T (2009) Explicit expressions for the Fréchet derivatives in 3D anisotropic resistivity inversion. *Geophysics* 74(3):F31–F43
- Griffiths D (1990) Failure criteria interpretation based on Mohr-Coulomb friction. *J Geotech Eng* 116(6):986–999
- Heise W, Caldwell T, Bibby H, Brown C (2006) Anisotropy and phase splits in magnetotellurics. *Phys Earth Planet Int* 158(2–4):107–121
- Herwanger J, Pain C, Binley A, De Oliveira C, Worthington M (2004) Anisotropic resistivity tomography. *Geophys J Int* 158(2):409–425
- Holder DS (2004) *Electrical impedance tomography: methods, history and applications*. CRC Press, Boca Raton
- Hoversten GM, Myer D, Key K, Alumbaugh D, Hermann O, Hobbet R (2015) Field test of sub-basalt hydrocarbon exploration with marine controlled source electromagnetic and magnetotelluric data. *Geophys Prospect* 63(5):1284–1310
- Jaeger J (1969) *Elasticity, fracture and flow* (3rd ed.). Methuen
- Jeong WC, Sajib SZ, Katoch N, Kim HJ, Kwon OI, Woo EJ (2017) Anisotropic conductivity tensor imaging of in vivo canine brain using DT-MREIT. *IEEE Trans Med Imaging* 36(1):124–131
- Jolly R, Sanderson D (1997) A Mohr circle construction for the opening of a pre-existing fracture. *J Struct Geol* 19(6):887–892
- Kirkby A, Heinson G (2015) Linking electrical and hydraulic conductivity through models of random resistor networks. *ASEG Ext Abstr* 2015(1):1–5
- Kirkby A, Heinson G (2017) Three-dimensional resistor network modeling of the resistivity and permeability of fractured rocks. *J Geophys Res: Solid Earth* 122(4):2653–2669
- Kirkby A, Heinson G, Krieger L (2016a) Relating electrical resistivity to permeability using resistor networks. *ASEG Ext Abstr* 2016(1):1–7
- Kirkby A, Heinson G, Krieger L (2016b) Relating permeability and electrical resistivity in fractures using random resistor network models. *J Geophys Res: Solid Earth* 121(3):1546–1564
- Kittel C (2005) *Introduction to solid state physics*, 8th edn. Wiley, New York
- Kozlovskaya E, Hjelt S-E (2000) Modeling of elastic and electrical properties of solid-liquid rock system with fractal microstructure. *Phys Chem Earth Part A* 25(2):195–200
- Kwon OI, Jeong WC, Sajib SZ, Kim HJ, Woo EJ (2014) Anisotropic conductivity tensor imaging in MREIT using directional diffusion rate of water molecules. *Phys Med Biol* 59(12):2955
- Labuz JF, Zang A (2012) Mohr-Coulomb failure criterion. *Rock Mech Rock Eng* 45(6):975–979

- Le G, Slavin J, Strangeway R (2010) Space technology 5 observations of the imbalance of regions 1 and 2 field-aligned currents and its implication to the cross-polar cap Pedersen currents. *J Geophys Res: Space Phys* 115(A07202)
- Li YG (2002) A finite-element algorithm for electromagnetic induction in two-dimensional anisotropic conductivity structures. *Geophys J Int* 148(3):389–401. <https://doi.org/10.1046/j.1365-246x.2002.01570.x>
- Lilley FEM (1976) Short note: diagrams for magnetotelluric data. *Geophysics* 41(4):766–770
- Lilley FEM (1993a) Magnetotelluric analysis using Mohr circles. *Geophysics* 58(10):1498–1506
- Lilley FEM (1993b) Mohr circles in magnetotelluric interpretation (i) simple static shift; (ii) Bahr's analysis. *J Geomagn Geoelectr* 45(9):833–839
- Lilley FEM (1998a) Magnetotelluric tensor decomposition: Part II. Examples of a basic procedure. *Geophysics* 63(6):1898–1907
- Lilley FEM (1998b) Magnetotelluric tensor decomposition: Part I, Theory for a basic procedure. *Geophysics* 63(6):1885–1897
- Lilley FEM (2012) Magnetotelluric tensor decomposition: insights from linear algebra and Mohr diagrams. In: Lim H-S (ed) *New achievements in geoscience*. InTech, London
- Lilley FE (2016) The distortion tensor of magnetotellurics: a tutorial on some properties. *Explor Geophys* 47(2):85–99
- Lilley FE (2018) The magnetotelluric tensor: improved invariants for its decomposition, especially 'the 7th'. *Explor Geophys* 49(5):622–636
- Løseth LO (2007) Modelling of controlled source electromagnetic data. Norwegian University of Science and Technology, Trondheim
- Löwer A, Junge A (2017) Magnetotelluric transfer functions: phase tensor and tipper vector above a simple anisotropic three-dimensional conductivity anomaly and implications for 3D isotropic inversion. *Pure Appl Geophys* 174(5):2089–2101
- Madden TR (1976) Random networks and mixing laws. *Geophysics* 41(6):1104–1125
- Maillet R (1947) The fundamental equations of electrical prospecting. *Geophysics* 12(4):529–556
- Makris J, Bogris N, Eftaxias K (1999) A new approach in the determination of characteristic directions of the geoelectric structure using Mohr circles. *Earth Planets Space* 51(10):1059–1065
- Mandolesi E (2013) Inversion of magnetotelluric data in an anisotropic domain. National University of Ireland, Galway
- Mandolesi E, Jones AG (2012) Magnetotelluric inversion in a 2D anisotropic environment. In: EGU general assembly conference abstracts, 2012 (vol 14, p 13561)
- Martí A (2014) The role of electrical anisotropy in magnetotelluric responses: from modelling and dimensionality analysis to inversion and interpretation. *Surv Geophys* 35(1):179–218
- Martí A, Queralt P, Ledo J, Farquharson C (2010) Dimensionality imprint of electrical anisotropy in magnetotelluric responses. *Phys Earth Planet Int* 182(3–4):139–151. <https://doi.org/10.1016/j.pepi.2010.07.007>
- Masahiko Takeda (1991) Role of Hall conductivity in the ionospheric dynamo. *J Geophys Res Space Phys* 96(A6):9755–9759
- McKeagney C, Boulter C, Jolly R, Foster R (2004) 3-D Mohr circle analysis of vein opening, Indarama lode-gold deposit, Zimbabwe: implications for exploration. *J Struct Geol* 26(6–7):1275–1291
- Meju, M. A., Saleh, A. S., Mackie, R. L., Miorelli, F., Miller, R. V., & Mansor, N. K. S. (2018). Workflow for improvement of 3D anisotropic CSEM resistivity inversion and integration with seismic using cross-gradient constraint to reduce exploration risk in a complex fold-thrust belt in offshore northwest Borneo. *Interpretation*, 6(3), SG49–SG57. doi:10.1190/int-2017-0233.1
- Miensepost MP, Jones AG (2011) Artefacts of isotropic inversion applied to magnetotelluric data from an anisotropic Earth. *Geophys J Int* 187(2):677–689
- Mogilatov V, Bespalov A (2009) Biaxial anisotropy in geoelectric prospecting. *Izvestiya Phys Solid Earth* 45(9):822–828
- Mohr O (1882) Ueber die Darstellung des Spannungszustandes und des Deformationszustandes eines Korperelementes und über die Anwendung derselben in der Festigkeitslehre. *Civilingenieur* 28:113–156
- Mollison, R., Schon, J., Fanini, O., Kreigshauser, B., Meyer, W., & Gupta, P. (1999) A model for hydrocarbon saturation determination from an orthogonal tensor relationship in thinly laminated anisotropic reservoirs. In: SPWLA 40th Annual Logging Symposium, 1999: Society of Petrophysicists and Well-Log Analysts
- Montgomery H (1971) Method for measuring electrical resistivity of anisotropic materials. *J Appl Phys* 42(7):2971–2975
- Moran J, Gianzero S (1979) Effects of formation anisotropy on resistivity-logging measurements. *Geophysics* 44(7):1266–1286

- Nekut AG (1994) Anisotropy induction logging. *Geophysics* 59(3):345–350
- Nye JF (1985) Physical properties of crystals: their representation by tensors and matrices. Oxford University Press, Oxford
- Okazaki T, Oshiman N, Yoshimura R (2016) Analytical investigations of the magnetotelluric directionality estimation in 1-D anisotropic layered media. *Phys Earth Planet Inter* 260:25–31
- Onwumechilli A (1967) Geomagnetic variations in the equatorial zone. In: *International geophysics*, vol 11. Elsevier, Amsterdam, pp 425–507
- Pain CC, Herwanger JV, Saunders JH, Worthington MH, de Oliveira CR (2003) Anisotropic resistivity inversion. *Inverse Prob* 19(5):1081
- Pek J, Santos FAM (2006) Magnetotelluric inversion for anisotropic conductivities in layered media. *Phys Earth Planet Inter* 158:139–158
- Pek J, Verner T (1997) Finite-difference modelling of magnetotelluric fields in two-dimensional anisotropic media. *Geophys J Int* 128:505–521. <https://doi.org/10.1111/j.1365-246X.1997.tb05314.x>
- Pervukhina M, Kuwahara Y, Ito H (2005) Fractal network and mixture models for elastic and electrical properties of porous rock. In: *Fractal behaviour of the earth system*. Springer, Berlin, pp 97–118
- Plotkin VV (2017) Method for determining the contribution of the Hall effect in magnetotelluric sounding. In: *Interexpo GEO-Siberia-2017. XIII Intern. scientific Congr (In Russian)*
- Pommier A (2014) Interpretation of magnetotelluric results using laboratory measurements. *Surv Geophys* 35(1):41–84
- Qin L, Yang C (2016) Analytic magnetotelluric responses to a two-segment model with axially anisotropic conductivity structures overlying a perfect conductor. *Geophys J Int* 205(3):1729–1739
- Qin L, Yang C, Chen K (2013) Quasi-analytic solution of 2-D magnetotelluric fields on an axially anisotropic infinite fault. *Geophys J Int* 192(1):67–74
- Rastogi RG, Chandra H (2006) Conductivity, electric field and electron drift velocity within the equatorial electrojet. *Earth, Planets and Space* 58(8):1071–1077
- Regis C, Rijo L (1997) 1-D inversion of anisotropic magnetotelluric data. In: *Extended abstracts book from the 50th congresso internacional da sociedade Brasileira de Geofísica, Brasil*, vol 2, pp 673–674
- Regis C, Rijo L (2000) Approximate equality constraints in the inversion of anisotropic MT data. In: *Abstracts book, 15th workshop on electromagnetic induction in the earth, Cabo Frio, Brazil*, p 47
- Rokityansky II (1982) Geoelectromagnetic fields. In: *Geoelectromagnetic investigation of the Earth's crust and mantle*. Springer, Berlin, pp 1–26
- Santos FAM, Mendes-Victor LA (2000) ID Anisotropic Versus 2D Isotropic Media In Magnetotellurics. *Acta Geodaetica et Geophysica Hungarica* 35(1):49–61
- Sarma S (1975) Seismic stability of earth dams and embankments. *Geotechnique* 25(4):743–761
- Sasaki Y (1994) 3-D resistivity inversion using the finite-element method. *Geophysics* 59(12):1839–1848
- Schmeling H (1986) Numerical models on the influence of partial melt on elastic, anelastic and electrical properties of rocks. Part II: electrical conductivity. *Phys Earth Planet Interiors* 43(2):123–136
- Schön JH (2015) Physical properties of rocks: fundamentals and principles of petrophysics (vol 65). Elsevier, Amsterdam
- Schön JH, Mollison R, Georgi D (1999) Macroscopic electrical anisotropy of laminated reservoirs: a tensor resistivity saturation model. In: *SPE annual technical conference and exhibition. Society of Petroleum Engineers*
- Schön JH, Georgi D, Fanini O (2000) Anisotropic reservoir characterization (laminated sands) using orthogonal resistivity, NMR, and formation test data. In: *EAGE conference on exploring the synergies between surface and borehole geoscience-petrophysics meets geophysics*
- Secor DT (1965) Role of fluid pressure in jointing. *Am J Sci* 263(8):633–646
- Semeriyarov F, Saphiannikova M, Heinrich G (2009) Anisotropic generalization of Stinchcombe's solution for the conductivity of random resistor networks on a Bethe lattice. *J Phys A: Math Theor* 42(46):465001
- Sen AK, Torquato S (1989) Effective conductivity of anisotropic two-phase composite media. *Phys Rev B* 39(7):4504
- Seo JK, Pyo HC, Park C, Kwon O, Woo EJ (2004) Image reconstruction of anisotropic conductivity tensor distribution in MREIT: computer simulation study. *Phys Med Biol* 49(18):4371
- Ugural AC, Fenster SK (2011) *Advanced mechanics of materials and applied elasticity*. Pearson Education
- Wang T, Fang S (2001) 3-D electromagnetic anisotropy modeling using finite differences. *Geophysics* 66(5):1386–1398
- Wannamaker PE (2005) Anisotropy versus heterogeneity in continental solid earth electromagnetic studies: fundamental response characteristics and implications for physicochemical state. *Surv Geophys* 26(6):733–765

- Weaver JT (2004) The use of Mohr circles in the interpretation of magnetotelluric data. ASEG Extended Abstracts 2004(1):1–4
- Weaver JT, Lilley F (2004) Using Mohr circles to identify regional dimensionality and strike angle from distorted magnetotelluric data. *Explor Geophys* 35(4):251–254
- Weidelt P, Oristaglio M, Spies B (1999) 3-D conductivity models: implications of electrical anisotropy. In: Oristaglio M, Spies B, Cooper MR (eds) *Three-dimensional electromagnetics*. Society of Exploration Geophysicists, Tulsa, pp 119–137
- Weiss CJ, Newman GA (2002) Electromagnetic induction in a fully 3-D anisotropic earth. *Geophysics* 67(4):1104–1114
- Wiese T, Greenhalgh S, Zhou B, Greenhalgh M, Marescot L (2015) Resistivity inversion in 2-D anisotropic media: numerical experiments. *Geophys J Int* 201(1):247–266
- Yang C (1997) MT numerical simulation of symmetrically 2D Anisotropic media based on the finite element method (in Chinese). *Northwest Seismol J* 19(2):27–33
- Yin C (2000) Geoelectrical inversion for 1D anisotropic models and inherent non-uniqueness. *Geophys J Int* 140:11–23
- Yin C (2003) Inherent nonuniqueness in magnetotelluric inversion for 1D anisotropic models. *Geophysics* 68(1):138–146
- Yin C, Weidelt P (1999) Geoelectrical fields in a layered earth with arbitrary anisotropy. *Geophysics* 64(2):426–434
- Yu L, Evans R, Edwards R (1997) Transient electromagnetic responses in seafloor with triaxial anisotropy. *Geophys J Int* 129(2):292–304
- Yuan N, Nie XC, Liu R, Qiu CW (2010) Simulation of full responses of a triaxial induction tool in a homogeneous biaxial anisotropic formation. *Geophysics* 75(2):E101–E114

Publisher's Note Springer Nature remains neutral with regard to jurisdictional claims in published maps and institutional affiliations.